REPORT R-445 NOVEMBER, 1969

CSL COORDINATED SCIENCE LABORATORY

INFLUENCE OF COLLISIONS ON THE INSTABILITY OF AN ELECTRON BEAM IN A PLASMA

M. RAETHER

UNIVERSITY OF ILLINOIS - URBANA, ILLINOIS

INFLUENCE OF COLLISIONS ON THE INSTABILITY OF AN ELECTRON BEAM IN A PLASMA

by

M. Raether

This work was supported in whole by the Joint Services Electronics Program (U.S. Army, U.S. Navy, and U.S. Air Force) under Contract DAAB 07-67-C-0199.

INFLUENCE OF COLLISIONS ON THE INSTABILITY OF AN ELECTRON BEAM IN A PLASMA

by

M. Raether

Abstract

This report contains a numerical and analytical study of the dispersion relation of a Lorentzian beam in a cold plasma with collisions. Numerical results for the growth rate, the mode structure and the group velocity are presented for selected parameters and analytical generalizations of these results are given, both for the case of real wavenumber and real frequency. In particular it is shown that in either case the high frequency instability is quenched for a sufficiently large velocity spread and collision frequency and that this quenching occurs over a much larger parameter range than has previously been assumed.

I. INTRODUCTION

The linear stage of the instability of a charged particle beam in a plasma without external magnetic field has been the subject of numerous theoretical investigations[1-15]. The influence of plasma temperature, beam temperature and finite geometry has been treated in considerable detail; the effect of collisions, however, has received comparatively little attention,[4,7-9] although it is of great practical importance in many experimental situations. As a consequence, a number of relevant questions connected with the influence of collisions have remained unanswered, and other points still require clarification. Examples for this are the modification of the mode structure by collisions, the simultaneous influence of velocity spread of the beam and collisions in the plasma and the collisional enhancement of the instability at low frequencies or wavenumbers.

In this report we present a numerical study of the effect of collisions on the instability of cold beams and beams with finite velocity spread interacting with a cold plasma in the absence of magnetic fields. The investigated parameter range was selected to correspond to experimental conditions of interest to us, the dimensionless formulation, however, allows, of course, to adapt the results to a wide range of experimental conditions. Some analytic generalizations that are presented should extend the usefulness of the results even further.

The following discussion is based on the dispersion relation of a Lorentzian beam in an infinite cold plasma with collisions. By cold plasma we mean in this context that we study a parameter range in which the thermal motion of the plasma electrons only enters in the collision frequency but does

not modify the plasma dynamics to any appreciable extent.

The choice of a Lorentzian beam is motivated by two considerations. First, a Lorentzian distribution function gives a simple algebraic dispersion relation which, in the situations that have been investigated, gives results that are very similar to those obtained from a displaced Maxwellian distribution[14,15]. Secondly, beams of finite velocity spread produced experimentally resemble more Lorentzian distributions than Maxwellians.[20,21] From the experimental point of view a displaced Maxwellian is therefore not necessarily preferable over any other reasonable one parameter distribution function. Moreover, in the parameter region of most practical interest, the results are relatively insensitive to the detailed shape of the distribution function so that the dispersion relation based on a Lorentzian beam distribution, despite its shortcoming as a genuine distribution function, can be considered a useful model equation to study the parameter dependence of the situations of interest.

The distribution function

$$f_o = \frac{\Delta v/\pi}{\Delta v^2 + (v-v_o)^2} \tag{1}$$

for the beam leads to the dispersion relation

$$1 = \frac{\omega_p^2}{\omega(\omega + i\nu_c)} - \frac{\omega_B^2}{[k\Delta v - i\,(\omega - kv_o)]^2} \tag{2}$$

ω_p and ω_B are the plasma frequencies of plasma and beam respectively, ν_c is the collision frequency. Only collision between plasma particles are taken into account, collision of beam particles with either each other or with plasma particles are negligible for low beam densities and high velocities. All

quantities are assumed to vary as $e^{i(kz - \omega t)}$. Upon introducing the dimensionless variables $x = \omega/\omega_p$, $\varkappa = \frac{kv_o}{\omega_p}$; $\alpha = \omega_B^2/\omega_p^2$, $\beta = \Delta v/v_o$, $\upsilon = \upsilon_c/\omega_p$ Equation 2 goes over into

$$1 = \frac{1}{x(x+i\upsilon)} - \frac{\alpha}{[\varkappa\beta - i(x-\varkappa)]^2} \tag{3}$$

In solving this dispersion relation we treat both the cases of real wavenumber and real frequency, the former being appropriate to the temporal development of the instability, the latter to the eventually resulting stationary state in a semi-infinite system or the injection of a premodulated beam into a plasma.

II. COLD BEAM WITH COLLISIONS

1. Real k, $\omega = \omega_r + i\gamma$: For $\beta = 0$, Equation 3 reduces to the well known dispersion relation for a cold beam

$$1 = \frac{1}{x(x+i\upsilon)} + \frac{\alpha}{(x-\varkappa)^2} \tag{4}$$

This equation has been discussed by Bludman, Watson and Rosenbluth.[4] They found that the largest growth rate occurs for $\varkappa \approx 1$; for small collision frequency $\upsilon_c \ll \gamma$, the maximum growth rate is essentially that for the collisionless case, namely

$$\gamma = \frac{\sqrt{3}}{2}\,\omega_p\,(\alpha/2)^{1/3} \tag{5}$$

For $\upsilon_c \gg \gamma$ collisions reduce the growth rate to

$$\gamma = \omega_p\,(\alpha/2\upsilon)^{\frac{1}{2}} \tag{6}$$

For low wavenumbers ($\varkappa \ll 1$), collisions enhance the instability and one finds for the growth rate

$$\gamma = \omega_p \, (\alpha \varkappa v/2)^{\frac{1}{2}} \tag{7}$$

A numerical solution of Equation 4 confirms these results and reveals a number of additional features of the instability.

Figure 1 shows a plot of the growth rate γ/ω as a function of $\varkappa$ for various values of v. α was kept constant = 10^{-4}. This value was chosen because it is representative of a typical experimental situation. We notice that with increasing collision frequency the maximum unstable wavenumber, which for the collisionless case is given by

$$k_{opt} = 1 + 3/2 \, (\alpha/2)^{2/3} \tag{8}$$

shifts to lower values. At the same time the unstable wavenumber range, which for the collisionless beam extends from $\varkappa = 0$ to $\varkappa = (1 + \alpha^{1/3})^{3/2}$, extends out to $\varkappa \to \infty$. The maximum growth rate goes asymptotically toward a constant value in the limit of large collision frequency. This asymptotic value is readily obtained from the dispersion relation in the limit $v \gg x$. Equation 4 then reduces to

$$1 = \frac{1}{ivx} + \frac{\alpha}{(x-\varkappa)^2}$$

On the unstable branch we put $x = \varkappa + \epsilon$ where $\epsilon \ll 1$ and obtain to lowest order in $\epsilon/\varkappa$

$$1 = -\frac{i}{v\varkappa} + \frac{\alpha}{\epsilon^2}$$

For the imaginary part of ϵ we find

$$\text{Im } \epsilon = (\alpha/2)^{\frac{1}{2}} \left\{ \frac{v\varkappa}{(1 + v^2\varkappa^2)^{\frac{1}{2}}} - \frac{v^2\varkappa^2}{1 + v^2\varkappa^2} \right\}^{\frac{1}{2}} \tag{9}$$

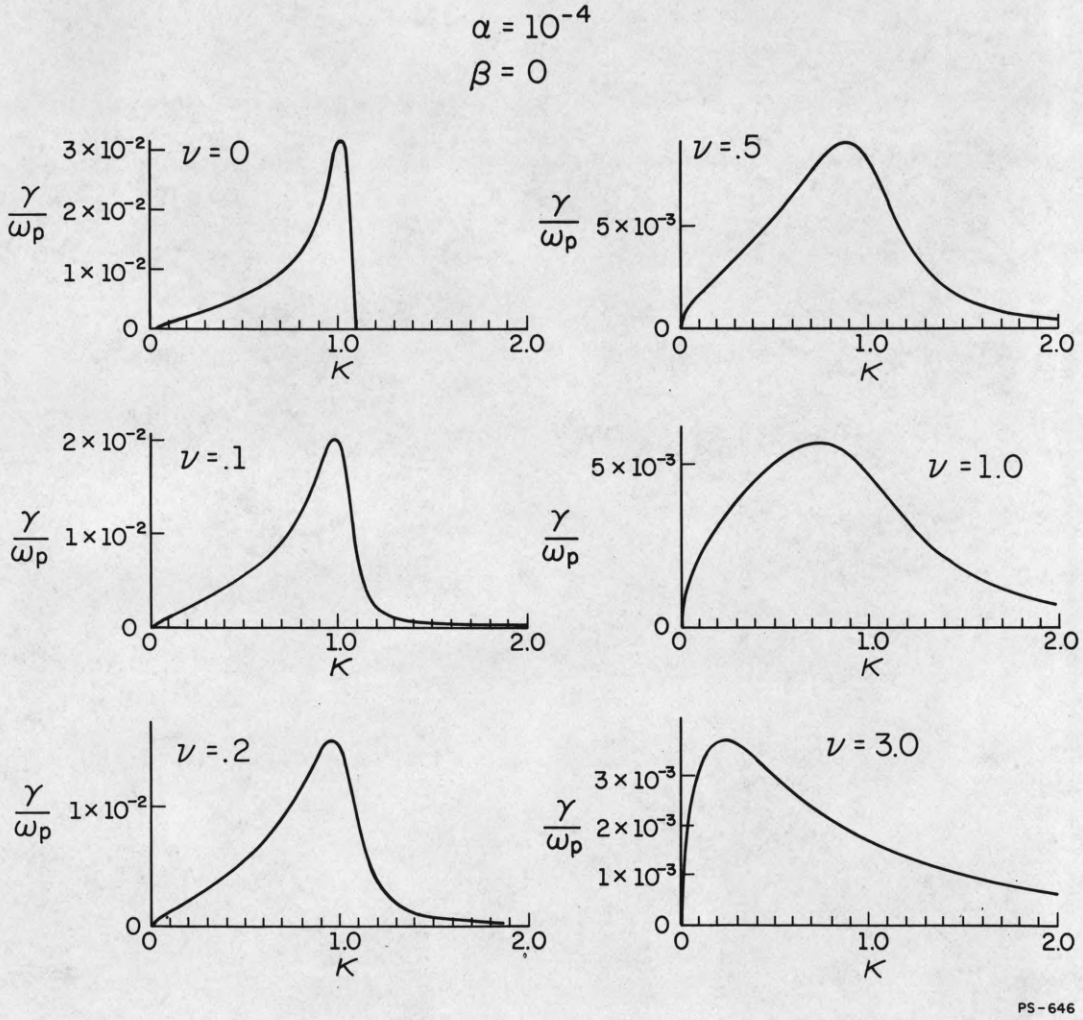

Figure 1. Cold-beam growth rate as a function of wave number for different collision frequencies.

The maximum growth rate follows from the condition

$$\frac{d\ \mathrm{Im}\ \epsilon}{d\varkappa} = 0$$

This condition is satisfied for $\varkappa_{opt} = \frac{1}{v\sqrt{3}}$; the growth rate follows as

$$(\mathrm{Im}\ \epsilon)_{opt} = \tfrac{1}{2}\ (\alpha/2)^{\frac{1}{2}} \tag{10}$$

In Figure 2 we have plotted the maximum growth rate as a function of collision frequency together with the approximate expression (5) (6) and (10). The large collision frequency approximation of BWR agrees to within 10% with the exact solution in the experimentally interesting region $0.1 < \nu < 0.5$. The breakdown of this approximation for larger ν is due to the fact that the maximum unstable $\varkappa$ shifts away from the assumed value $\varkappa = 1$. This behavior is shown in Figure 3 where $\varkappa_{opt}$ is plotted versus ν together with the approximate expression for small and large collision frequency.

Figure 4 shows a plot of the real and imaginary parts of the roots of Equation 2 in the neighborhood of $\varkappa = 1$, with ν as a parameter. The picture is reminiscent of the behavior of a warm beam without collision as discussed by O'Neil and Malmberg[14]. The essential difference is that the unstable root is always located on the "slow beam-branch".

An interesting consequence of this is, that the harmonics of the plasma frequency can become unstable in the presence of collision since the unstable k-range now extends to infinity. This may have consequences for wave-wave coupling processes during the nonlinear phase of the instability. A small velocity spread, however, decreases the unstable range and the second harmonic may become damped.

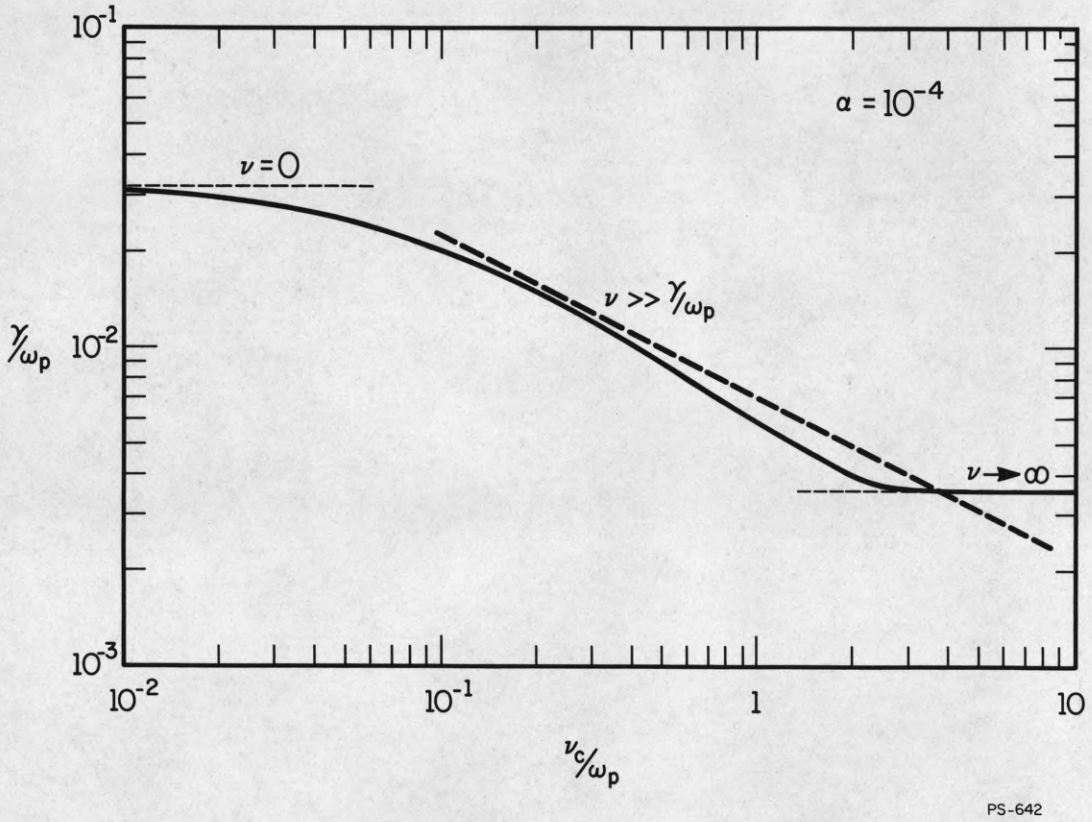

Figure 2. Maximum growth rate as a function of collision frequency.

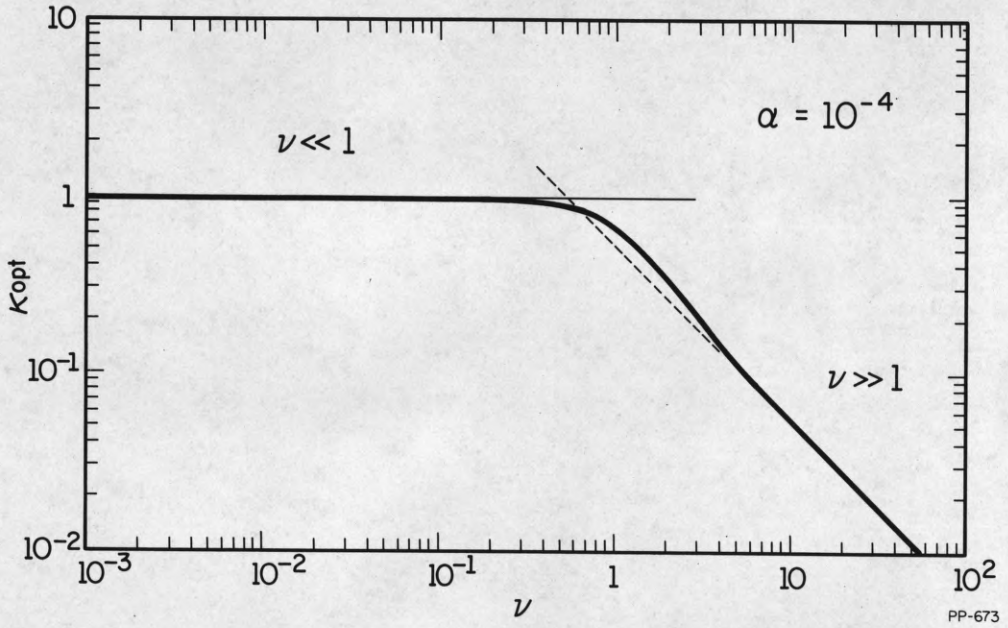

Figure 3. Wave number at maximum growth rate as a function of collision frequency.

$\alpha = 10^{-4}$

$\beta = 0$

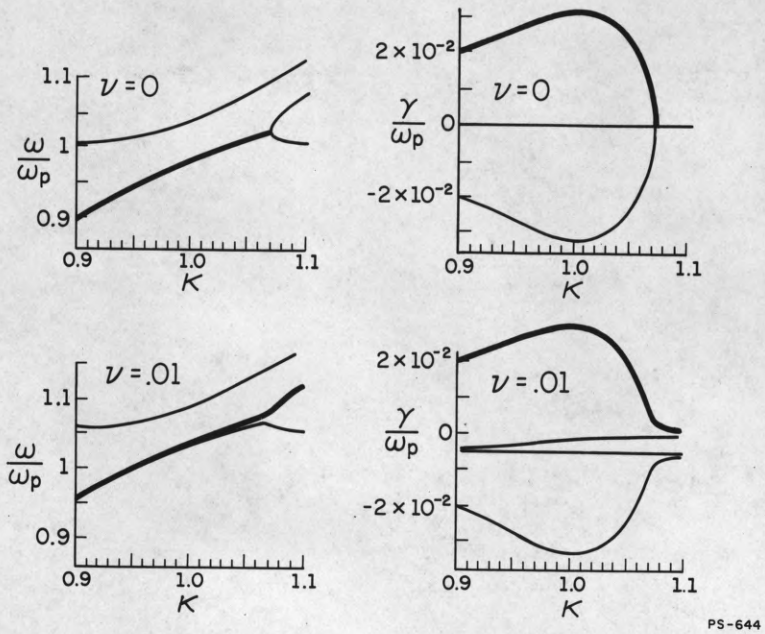

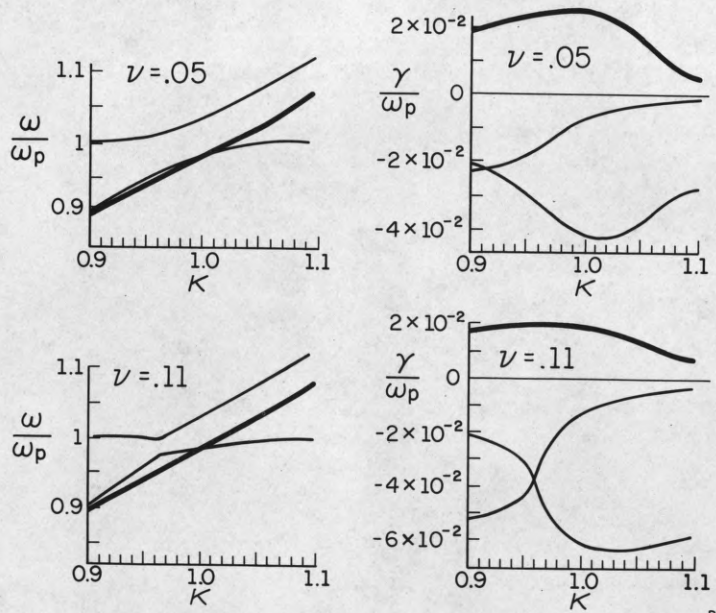

Figure 4a. Real and imaginary part of the frequency as a function of wave number for different collision frequencies. The heavy lines corresponds to the unstable mode.

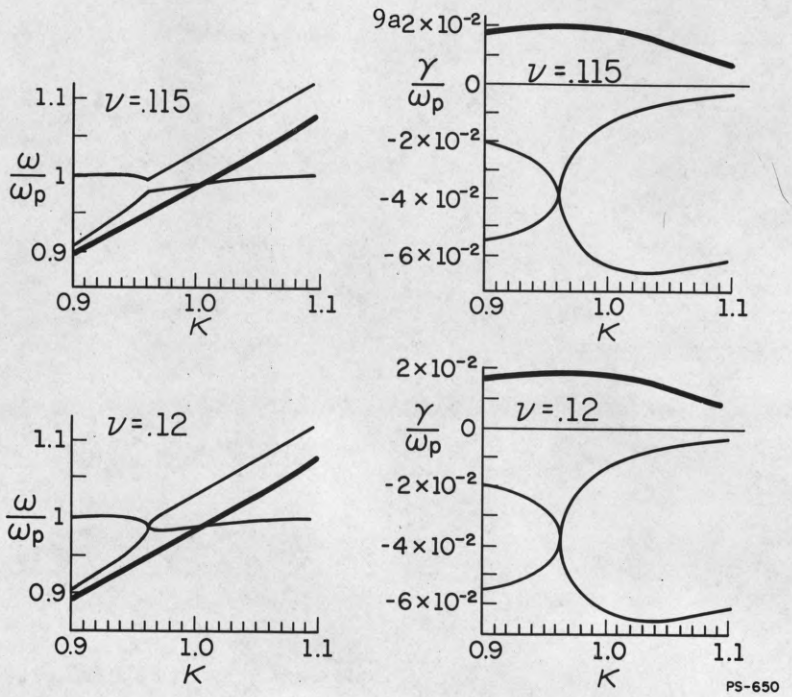

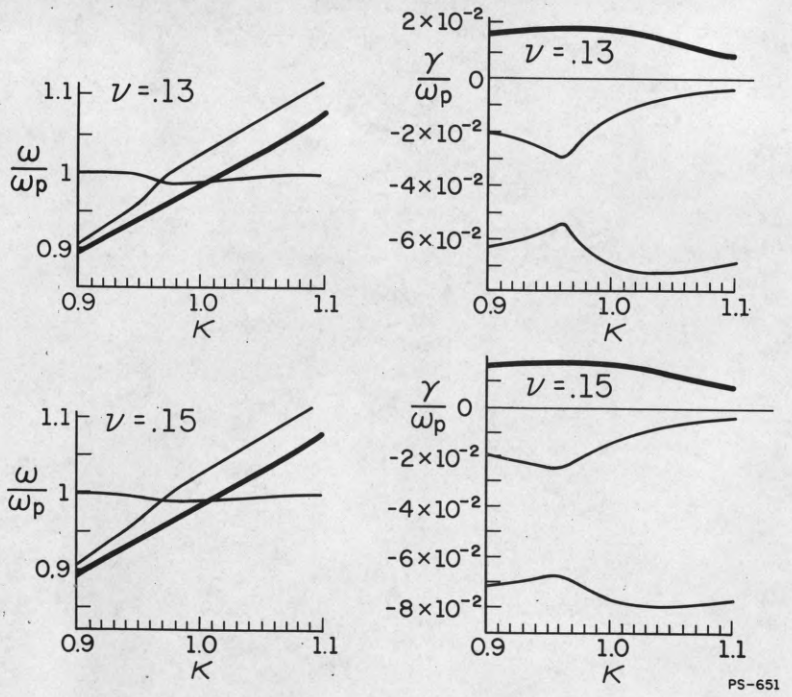

Figure 4b. Real and imaginary part of the frequency as a function of wave number for different collision frequencies. The heavy lines corresponds to the unstable mode.

Although the present example refers to only one particular value of α, it follows from the deviation of Equation 6 that is the neighborhood of $\varkappa = 1$, $\gamma/\omega_p\nu$ is a universal function of α/ν^3.

The physical mechanism of the low frequency instability can be understood easily if we observe that for $\nu_c \gg \omega$ the equation of motion for the plasma electron gives a pure viscous drift velocity of

$$v_D = \frac{e}{m} E/\nu_c \tag{11}$$

Consider a charge perturbation of wavelength λ on the beam. The electric field associated with a charge density n_B is $E \approx 4\pi\, en_B\, \lambda$. This field gives rise to a drift velocity of the plasma electron of

$$v_D = \frac{e}{m} \frac{4\pi\, en_B\, \lambda}{\nu_c}$$

The plasma electrons move in such a fashion as to compensate the beam space charge. The time necessary to do this is

$$\tau = \frac{n_B \lambda}{v_D n_p} = \nu_c/\omega_p{}^2 \tag{12}$$

The fraction n_B/n_p appears because only this fraction of the plasma electron is necessary for space charge neutralization. If this time is equal to $\frac{1}{\omega}$ the neutralizing space change is just out of phase with the perturbation and the original perturbation is enhanced. This gives the instability condition $\tau = \frac{\nu_c}{\omega_p{}^2} = \frac{1}{\omega} = \frac{1}{kv_o}$ or $\nu k = 1$ which is of the correct order of magnitude. The low frequency instability can therefore be classified as a viscous drag instability, similar in nature to the hose instability[16-17].

2. Real ω, $k = k_r + i\sigma$: For a beam in a cold collisionless plasma the imaginary part of k becomes infinite for $\omega = \omega_p$ and no stationary state is possible within the linear regime. This divergence is removed by either including collisions or a finite plasma temperature. We shall assume in the following that collisions dominate over the temperature effect and discuss later the conditions under which this is true.

The dispersion relation

$$1 = \frac{1}{x(x + i\nu)} + \frac{\alpha}{(x-\varkappa)^2}$$

can immediately be solved for $\varkappa$ to give

$$\varkappa_r = x \pm (\alpha/2)^{\frac{1}{2}} \left(- \frac{A}{B} + \frac{1}{B^{\frac{1}{2}}}\right)^{\frac{1}{2}}$$

(13)

$$\frac{\sigma v_o}{\omega_p} = \mp (\alpha/2)^{\frac{1}{2}} \left(\frac{A}{B} + \frac{1}{B^{\frac{1}{2}}}\right)^{\frac{1}{2}}$$

with

$$A = \frac{1}{x^2 + \nu^2} - 1$$

$$B = \left(\frac{1}{x^2 + \nu^2} - 1\right)^2 + \frac{\nu^2/x^2}{(x^2 + \nu^2)^2}$$

We note that a negative imaginary $\varkappa$ corresponds to growing waves propagating in the positive z-direction. For the high frequency mode the maximum spatial growth will occur in the vicinity of $x = 1$. We therefore put $x^2 = 1 + \epsilon$ and obtain to lowest order in ϵ and ν.

(14)
$$\frac{\sigma v_o}{\omega_p} = (\alpha/2)^{\frac{1}{2}} \left(\frac{-\epsilon}{\epsilon^2 + \nu^2} + \frac{1}{\epsilon^2 + \nu^2)^{\frac{1}{2}}} \right)^{\frac{1}{2}}$$

The condition for maximum spatial growth $\frac{d\sigma}{d\epsilon} = 0$ gives

(15)
$$\epsilon = - \nu/3^{\frac{1}{2}}$$

With this value for ϵ we obtain

$$\frac{v_o}{\omega_p}\,\sigma_{opt} = -\frac{3^{3/4}}{2}\,(\alpha/2\upsilon)^{\frac{1}{2}} \tag{16}$$

and

$$x_{opt} = 1 - \tfrac{1}{2}\,\upsilon/3^{\frac{1}{2}} + O(\upsilon^2) \tag{17}$$

$$\kappa_{opt} = 1 - \tfrac{1}{2}\,\upsilon/\sqrt{3} + 3^{\frac{1}{4}}/2\,(\alpha/2\upsilon)^{\frac{1}{2}} + O(\upsilon^2)$$

We are now in a position to discuss the relative importance of collisions and plasma temperature on the spatial growth. The inclusion of plasma temperature leads to the dispersion relation

$$1 = \frac{\omega_p^2}{\omega(\omega + i\upsilon_c) - k^2 v_e^2} + \frac{\omega_B^2}{(\omega - kv_o)^2}\;; \qquad v_e^2 = \frac{3T}{m} \tag{18}$$

Comparing the imaginary parts in the denominator of the first term on the r.h.s. we obtain the condition for collisions to dominate as

$$\upsilon_c\,\omega \gg 2\,k_r\,\sigma\,v_e^2 \tag{19}$$

With the value for σ from Equation 16 this becomes

$$\frac{v_e^2}{v_o^2} \ll \frac{\upsilon^{3/2}}{\alpha^{\frac{1}{2}}}\,\frac{\sqrt{2}}{3^{3/4}} \tag{20}$$

For very small values of υ ($\upsilon \ll \alpha$) k_r becomes comparable to σ and the criterium (20) takes the form

$$\frac{v_e^2}{v_o^2} \ll \frac{8}{3^{3/2}}\,\frac{\upsilon^2}{\alpha} \tag{20a}$$

It follows that for high energy, low density beams, collisions are almost always the dominate factor in limiting the spatial growth.

The frequency dependence of the spatial growth rate is shown in Figure 5 for selected collision frequencies. Similar to the case of real $\varkappa$, the maximum unstable frequency shifts to lower values with increasing collision frequency, thus invalidating the assumption $x \approx 1$. In Figure 6, the maximum spatial growth rate is plotted versus collision frequency. For large ν, σ goes towards a constant value. The analogy with the real $\varkappa$ case follows immediately if we take the limit of large ν in Equation 4. We obtain

$$\frac{\sigma v_o}{\omega_p} = -(\alpha/2)^{\frac{1}{2}} \left(\frac{1}{(1 + \frac{1}{\nu^2 x^2})^{\frac{1}{2}}} - \frac{1}{(1 + \frac{1}{\nu^2 x^2})} \right)^{\frac{1}{2}} \tag{21}$$

This is of the same form as Im x for $\varkappa$ real with x and $\varkappa$ interchanged. We therefore have maximum growth for $x = \frac{1}{\nu\sqrt{3}}$ and the limiting spatial growth rate becomes

$$\frac{\sigma v_o}{\omega_p} = 1/2 \; (\alpha/2)^{\frac{1}{2}} \tag{22}$$

In this limit the Im k and the Im ω are connected via the simple relation

$$\text{Im } \omega = v_o \text{ Im } k \tag{23}$$

III. SIMULTANEOUS ACTION OF COLLISIONS AND VELOCITY SPREAD

1. Reak k: The effect of a velocity spread on the instability of a Lorentzian beam in the absence of collisions has been treated extensively by O'Neil and Malmberg[14]. The somewhat surprising result of their work is that for a critical velocity spread the unstable mode shifts from the "beam-branch" to the "plasma branch" of the dispersion relation. If collisions are present in addition to a velocity spread the question arises as to how the transition from the unstable beam branch to the unstable plasma branch proceeds when the

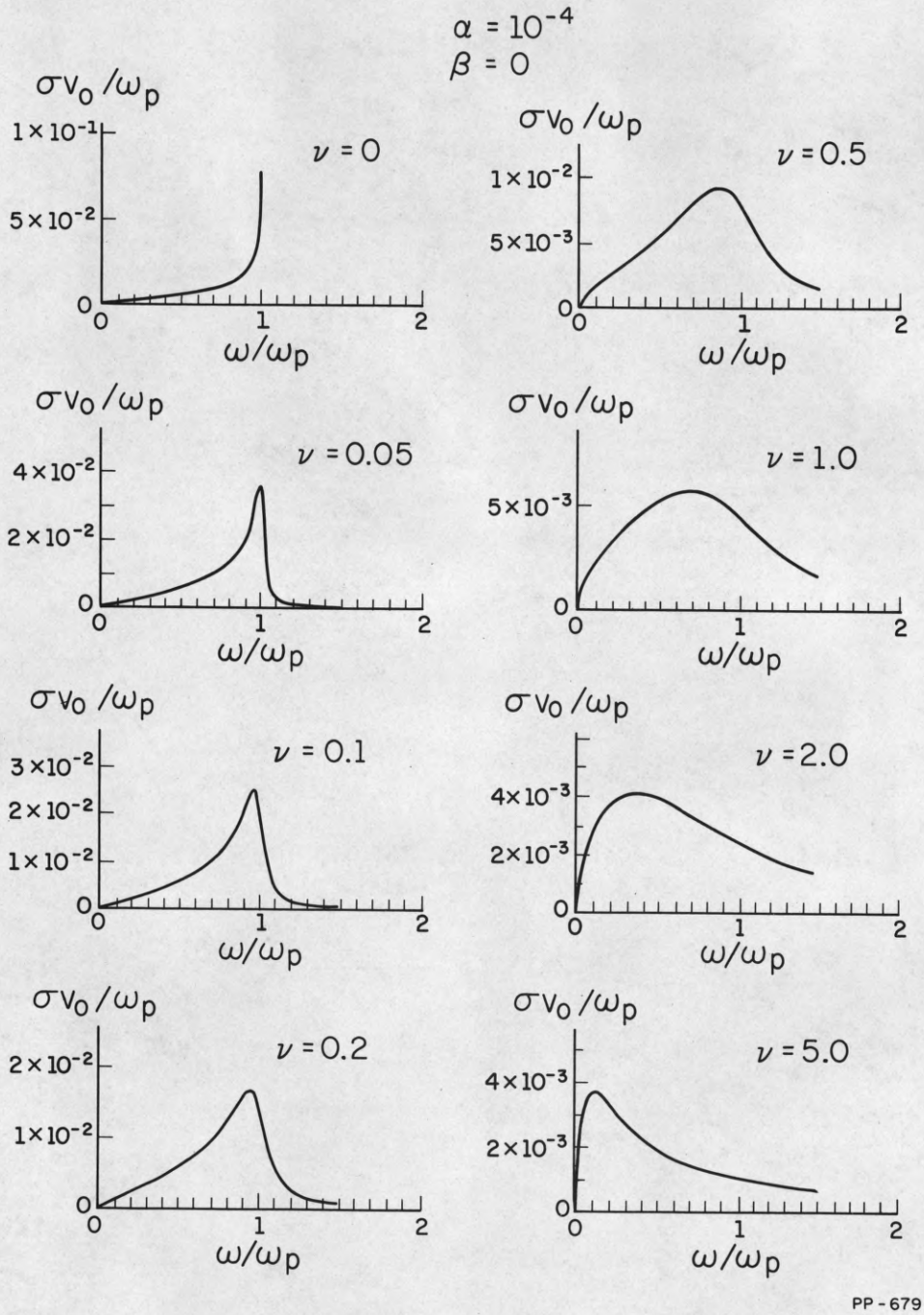

Figure 5. Spatial growth rate as a function of frequency for different collision frequencies.

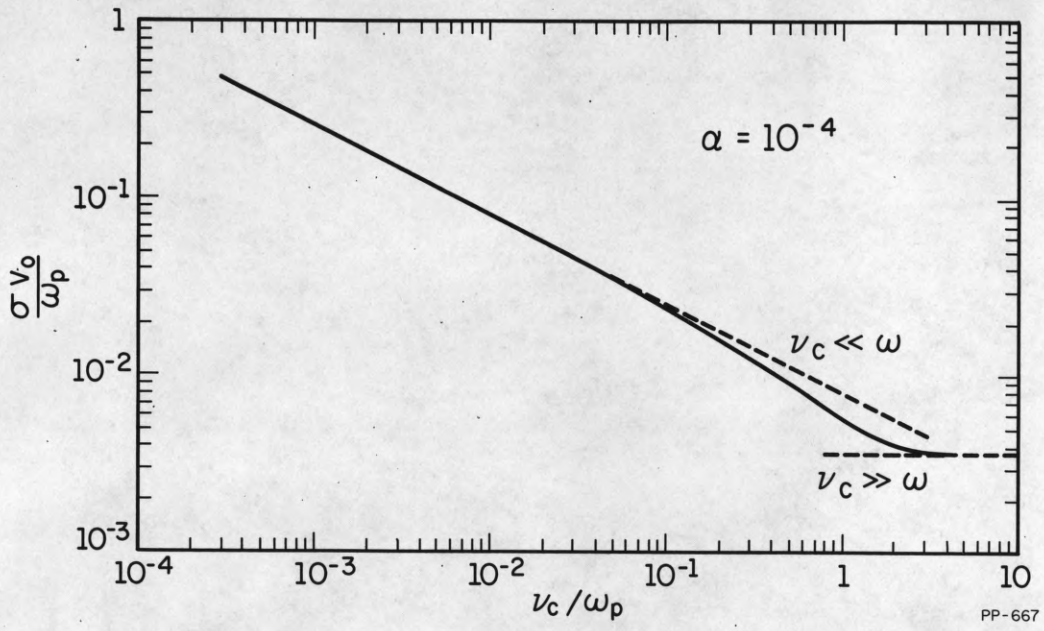

Figure 6. Maximum spatial growth rate as a function of collision frequency.

system goes from a collision dominated to a velocity spread dominated situation. Figure 7 shows as an example for $\alpha = 10^{-4}$, $\nu = 0.01$. As the velocity spread is "turned on", the unstable region on the beam branch shrinks from $\varkappa = \infty$ to a finite value $\varkappa_{max}$. With increasing velocity spread $\varkappa_{max}$ decreases until for $\beta \approx \nu/2$ the roots of the dispersion relation take on a shape reminiscent of the cold beam dispersion relation except that all roots are offset by $-i\nu/2$. If the velocity spread is increased further the unstable mode shifts over to the plasma branch and the subsequent behavior is qualitatively similar to the collisionless case.

The degeneracy point, where the unstable mode switches branches, can be obtained analytically in the following way:

If we introduce $x' = x + i\,\frac{\nu}{2}$ as a new variable, Equation 3 goes over into

$$1 = \frac{1}{x'^2 + \frac{1}{4}\nu^2} - \frac{\alpha}{\left[\varkappa\beta - \frac{\nu}{2} + i\,(\varkappa - x')\right]^2} \tag{24}$$

For $\frac{\nu}{2} = \varkappa\beta$ and $\nu^2 \ll x^2$ this has the same form as the cold beam dispersion relation without collisions. The degeneracy point is given by $\varkappa_{max} = (1 + \alpha^{1/3})^{3/2}$ and in the vicinity of this point we expect $x'(\varkappa)$ to be the same as $x(\varkappa)$ for the cold collisionless beam.

The velocity spread has moreover the effect of splitting the instability into two distinct modes, one at high and one at low frequencies. This is particularly noticable at higher collision frequencies. Figure 8 shows an example for this behavior. These two modes behave differently as a function of velocity spread. Whereas the low frequency mode has always finite, though small, growth rates, the high frequency mode damps out above

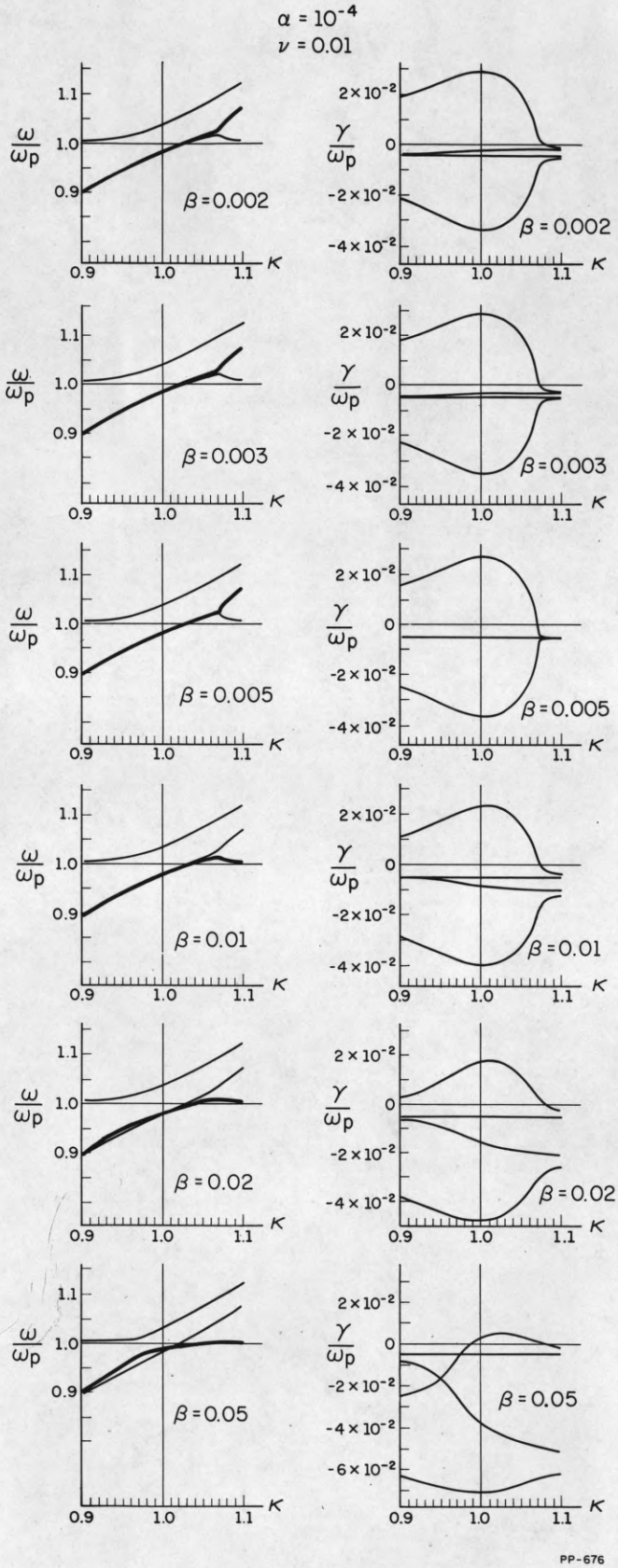

Figure 7a. Real and imaginary part of the frequency as a function of wave number for different velocity spreads. The collision frequency is constant = 0.01 ω_p. The heavy line corresponds to the unstable mode.

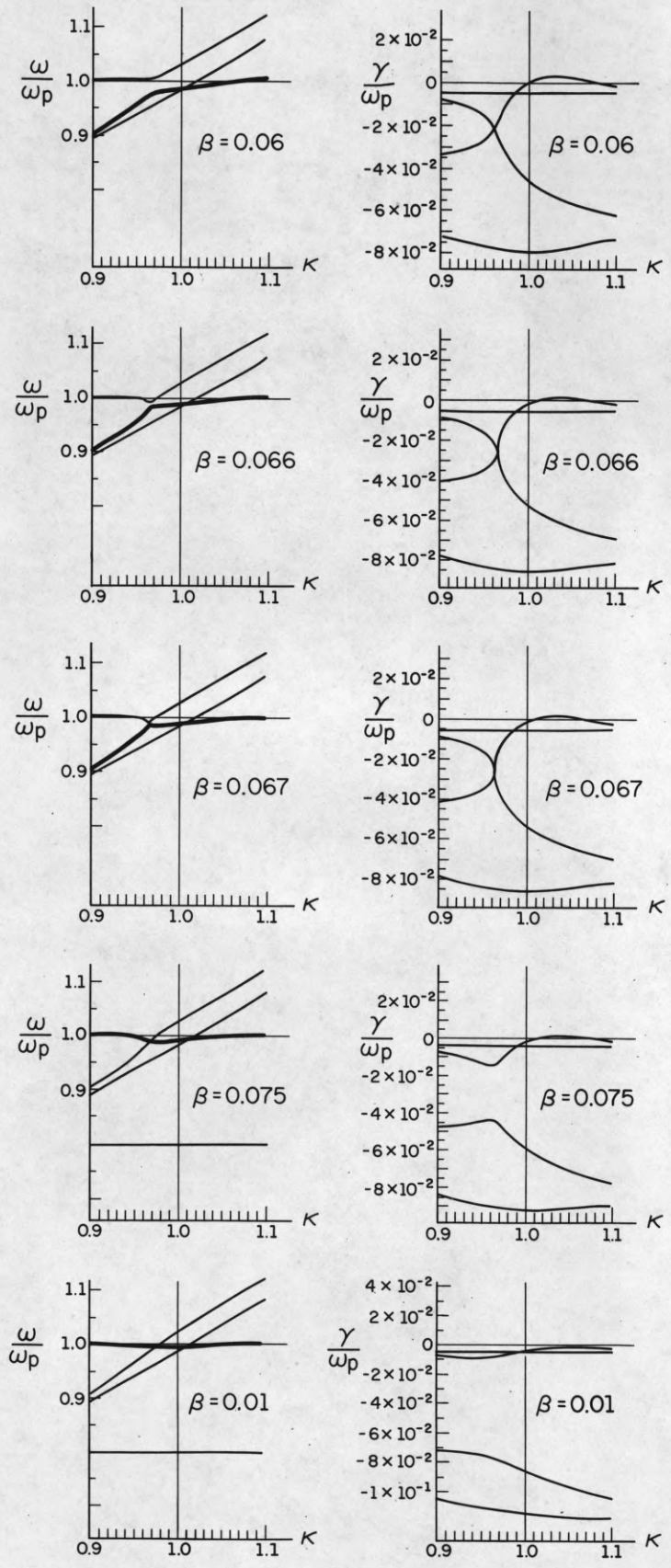

Figure 7b. Real and imaginary part of the frequency as a function of wave number for different velocity spreads. The collision frequency is constant = 0.01 ω_p. The heavy line corresponds to the unstable mode.

$\alpha = 10^{-4}$

$\nu = 0.3$

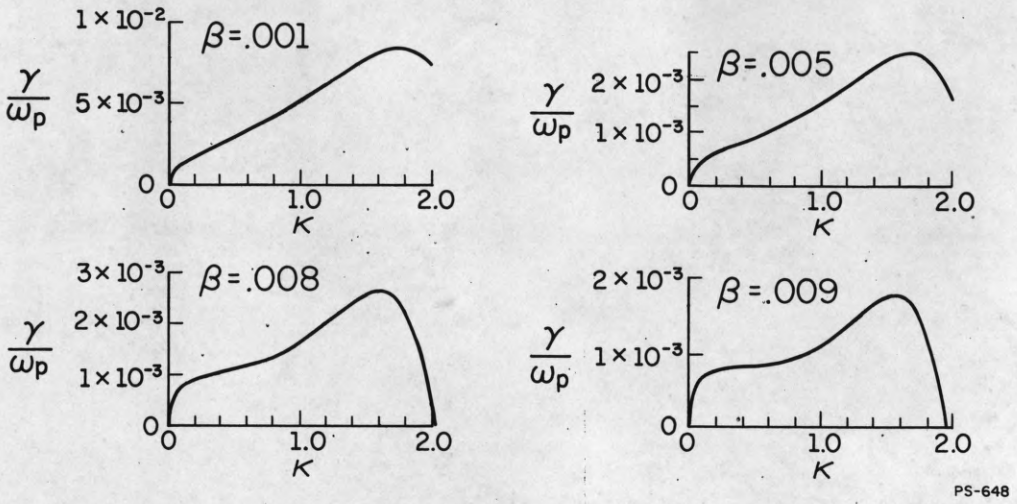

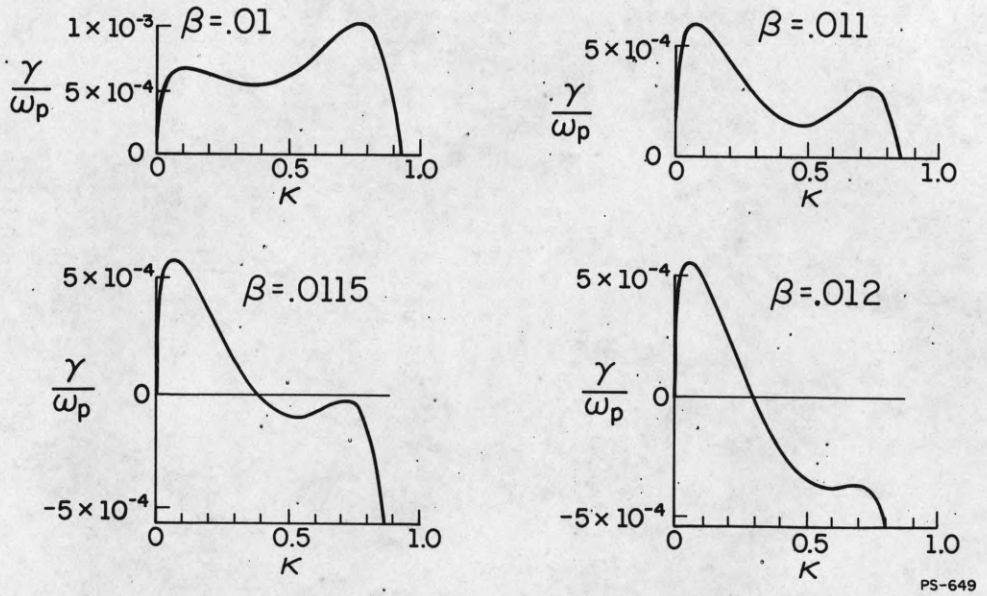

Figure 8. Growth rate as a function of wave number for different velocity spread at constant collision frequency.

a certain critical velocity spread. This quenching of the high frequency mode was first noticed by Ascoli[8]. For a beam with a displaced Maxwellian distribution function of r.m.s. width Δv, Ascoli found that collisions can quench the high frequency instability provided that

$$\upsilon > \sqrt{\frac{\pi}{2e}} \cdot \alpha \left(\frac{v_o}{\Delta v}\right)^2 \tag{25}$$

and

$$\frac{\Delta v}{v_o} \gg \alpha^{1/3} \tag{26}$$

The last condition requires that the beam is "warm", or in other words, that the interaction is resonant.

Based on numerical calculations Singhaus[9] gives the criterium, for quenching as

$$\upsilon > 0.66 \cdot \alpha \left(\frac{v_o}{\Delta v}\right)^2 \tag{27}$$

in close agreement with the value of Ascoli.

In Figure 9 we have plotted the maximum growth rate as a function of υ and β for $\alpha = 10^{-4}$. We see that the criterium given by Singhaus agrees very well with the zero growth rate contour and that it is actually valid for much lower velocity spreads than the condition $\beta \gg \alpha^{1/3}$ would indicate. The reason for this is, that the criterium for the interaction to be resonant, changes when collisions become important. This can be seen as follows:

For a cold beam in a collisionless plasma the frequency and wavenumber of the most unstable mode is given up to terms of order $\alpha^{1/3}$ by

$$\omega = \omega_p \left(1 - \tfrac{1}{2} (\alpha/2)^{1/3}\right)$$

$$k = \frac{\omega_p}{v_o}$$

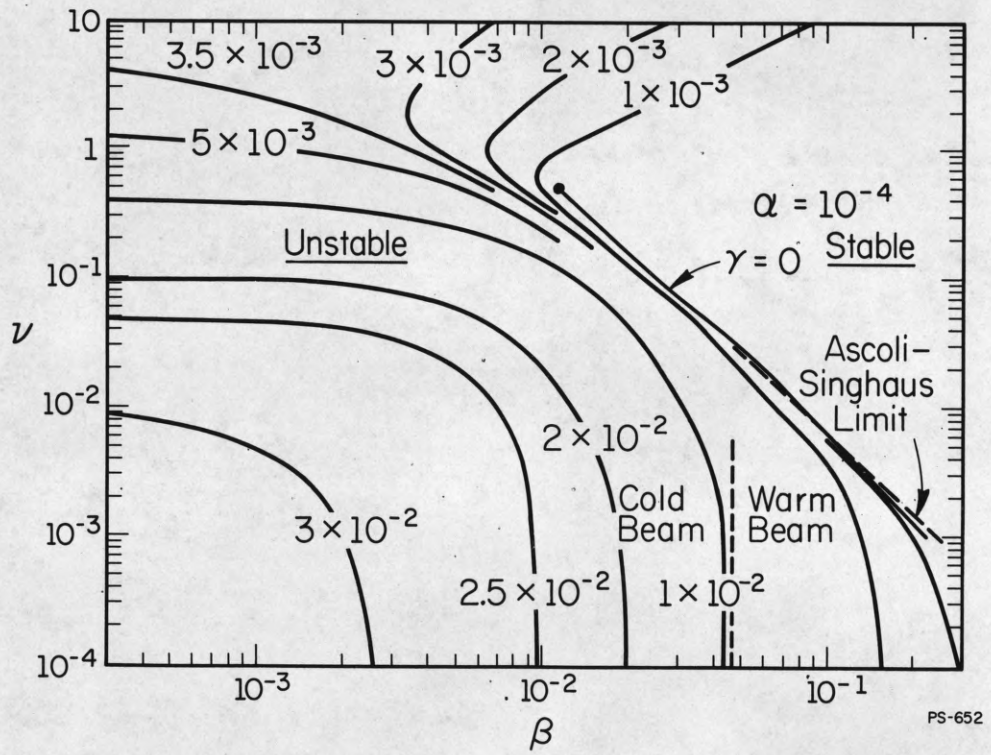

Figure 9. Contours of maximum growth rate in a ν-β-diagram. The line separating the cold beam and the warm beam region is given by $\beta = \alpha^{1/3}$.

We therefore obtain for the phase velocity

$$v_{ph} = \frac{\omega}{k} = v_o \left(1 - \tfrac{1}{2} (\alpha/2)^{1/3}\right) \tag{28}$$

Since the phase velocity is less than the beam velocity there are no beam particles with velocities equal to the phase velocity of the wave and the interaction is non-resonant. For resonant interaction to occur we must require that the velocity distribution of the beam particles is spread out over a velocity region of the order

$$\Delta v = v_o - v_{ph}$$

This condition immediately gives the criterium

$$\beta = \Delta v / v_o = \frac{1}{2^{4/3}} \alpha^{1/3} \tag{29}$$

in agreement with Equation 26. Δv is now a suitable measure for the width of the distribution function.

In the presence of collisions we have in the region of intermediate collision frequency ($\nu_c \gg \gamma$)

$$\omega = \omega_p \left(1 - (\alpha/2\nu)^{\frac{1}{2}}\right)$$

$$k \approx \omega_p / v_o$$

and

$$v_{ph} = \frac{\omega}{k} = v_o \left(1 - (\alpha/2\nu)^{\frac{1}{2}}\right) \tag{30}$$

Applying the same arguments as above we obtain the condition for resonant interaction as

$$\beta > (\alpha/2\nu)^{\frac{1}{2}} \tag{31}$$

This relation is very nearly the same as the Ascoli-Singhaus criterium for stability. We can therefore conclude that for parameters for which the

instability becomes resonant in the collision dominated regime, the instability is also quenched so that a resonant instability is not possible.

Resonant interaction with non-zero growth rate can only occur when

$$\nu_c \ll \gamma$$

or

$$\nu_c \ll \frac{\sqrt{3}}{2} (\alpha/2)^{1/3} \omega_p \tag{32}$$

The regions of resonant and non-resonant interaction are shown schematically in Figure 10.

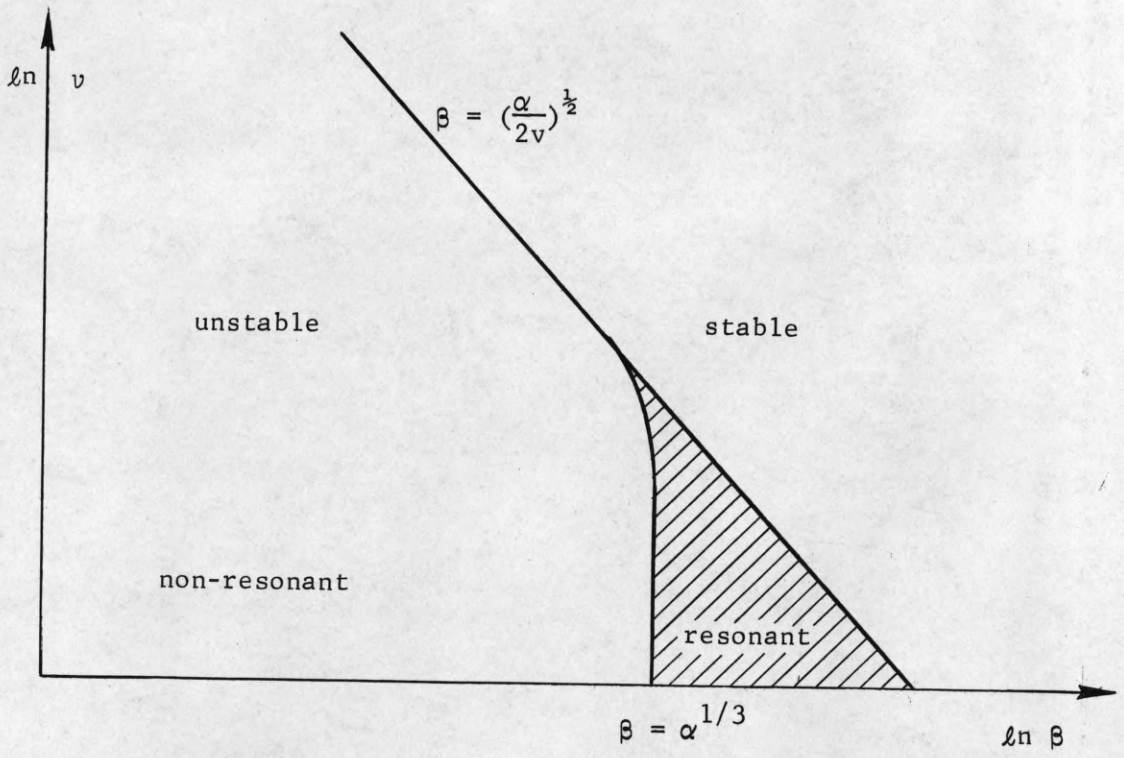

Figure 10. Schematic diagram of the regions of resonant and non-resonant interaction.

For collision frequencies $\nu > 0.6$ the distinction between low and high frequencies mode loses its meaning, there is a continuous shift from high to low frequency as β is increased.

This behavior is further illustrated in Figure 11 where the unstable wavenumber range is plotted as a function of β for different values of ν as a parameter.

We note that the low frequency mode is always present for finite collision frequency although it is restricted to a very small wavenumber range.

2. Real ω: For real frequency we obtain from Equation 3

$$\varkappa_r = \frac{1}{1+\beta^2}\left\{x \pm (\alpha/2)^{\frac{1}{2}}\left[-\frac{A}{B}+\frac{1}{\sqrt{B}}\right]^{\frac{1}{2}} \pm (\alpha/2)^{\frac{1}{2}}\beta\left[\frac{A}{B}+\frac{1}{\sqrt{B}}\right]^{\frac{1}{2}}\right\}$$

$$\frac{\sigma v_o}{\omega_p} = \frac{1}{1+\beta^2}\left\{\mp (\alpha/2)^{\frac{1}{2}}\left[\frac{A}{B} \pm \frac{1}{\sqrt{B}}\right]^{\frac{1}{2}} + \beta x \pm (\alpha/2)^{\frac{1}{2}}\beta\left[-\frac{A}{B}+\frac{1}{\sqrt{B}}\right]^{\frac{1}{2}}\right\}$$

For the high frequency mode we put again

$$x^2 = 1 + \epsilon$$

to obtain

$$\sigma v_o/\omega_p = \frac{1}{1+\beta^2}\left\{-(\alpha/2)^{\frac{1}{2}}\left[-\frac{\epsilon}{\epsilon^2+\nu^2}+\frac{1}{(\epsilon^2+\nu^2)^{\frac{1}{2}}}\right]^{\frac{1}{2}}\right.$$
$$\left. + \beta\left[1+\frac{\epsilon}{2} \pm (\alpha/2)^{\frac{1}{2}} \times \left[\frac{\epsilon}{\epsilon^2+\nu^2}+\frac{1}{(\epsilon^2+\nu^2)^{\frac{1}{2}}}\right]\right]\right\} \tag{34}$$

If the velocity spread and the collision frequency are not too large, ϵ is of order ν and we may neglect the last two terms in the last bracket and therefore have approximately

$$\frac{\sigma v_o}{\omega_p} = -\frac{1}{1+\beta^2}\left[(\alpha/2)^{\frac{1}{2}}\left(\frac{-\epsilon}{\epsilon^2+\nu^2}+\frac{1}{\epsilon^2+\nu^2)^{\frac{1}{2}}}\right)^{\frac{1}{2}} - \beta\right], \tag{35}$$

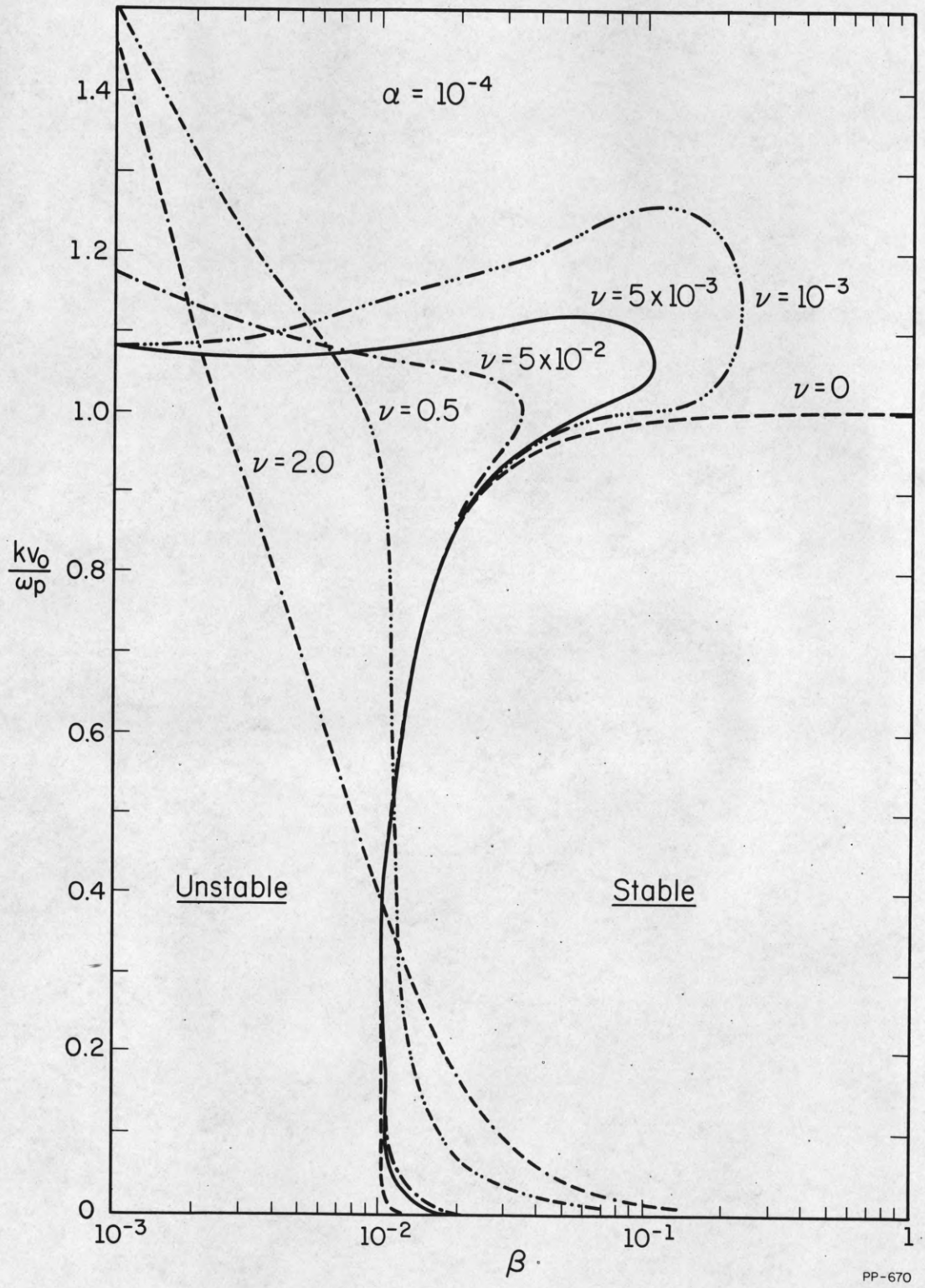

Figure 11. Contours of zero growth rate in a ν-β-diagram.

Maximum growth occurs again for $\epsilon = -\nu/\sqrt{3}$ and we find

$$\frac{\sigma v_o}{\omega_p} = -\frac{1}{1+\beta^2}\left[\frac{3^{3/4}}{2}(\alpha/2\nu)^{\frac{1}{2}} - \beta\right] \tag{36}$$

Similar to the case of real k complete quenching of the instability occurs for

$$\nu > \frac{3^{3/2}}{8}\frac{\alpha}{\beta^2} = 0.65\,\frac{\alpha}{\beta^2} \tag{37}$$

This criterium is very nearly the same as that given by Singhaus.

In Figure 12 we have plotted the maximum spatial growth rate in a ν - β - diagram. The contour of zero growth rate agrees very well with the approximate analytical expression of Equation 37.

The frequency dependence of the growth rate is demonstrated in Figure 13. Again a splitting into a high and a low frequency mode occurs and the picture is qualitatively similar to the real k case.

Figure 14 shows the corresponding x - β diagram with the contours of equal growth rate.

The criterium for transition from non-resonant to resonant interaction can easily be given for the practically interesting region where $(\alpha/2\nu)^{\frac{1}{2}} \ll 1$. We found for the most unstable mode

$$\omega = \omega_p\,(1 - \frac{\nu}{2\sqrt{3}}) \tag{38}$$

$$k = \omega_p/v_o\,(1 - \frac{\nu}{2\sqrt{3}} + \frac{3^{\frac{1}{4}}}{2}(\alpha/2\nu)^{\frac{1}{2}}) \tag{39}$$

The phase velocity becomes

$$v_{ph} = v_o\,(1 - \frac{3^{\frac{1}{4}}}{2}(\alpha/2\nu)^{\frac{1}{2}}) \tag{40}$$

We require again that the velocity spread of the beam overlaps the phase velocity and arrrive at the condition for resonant coupling

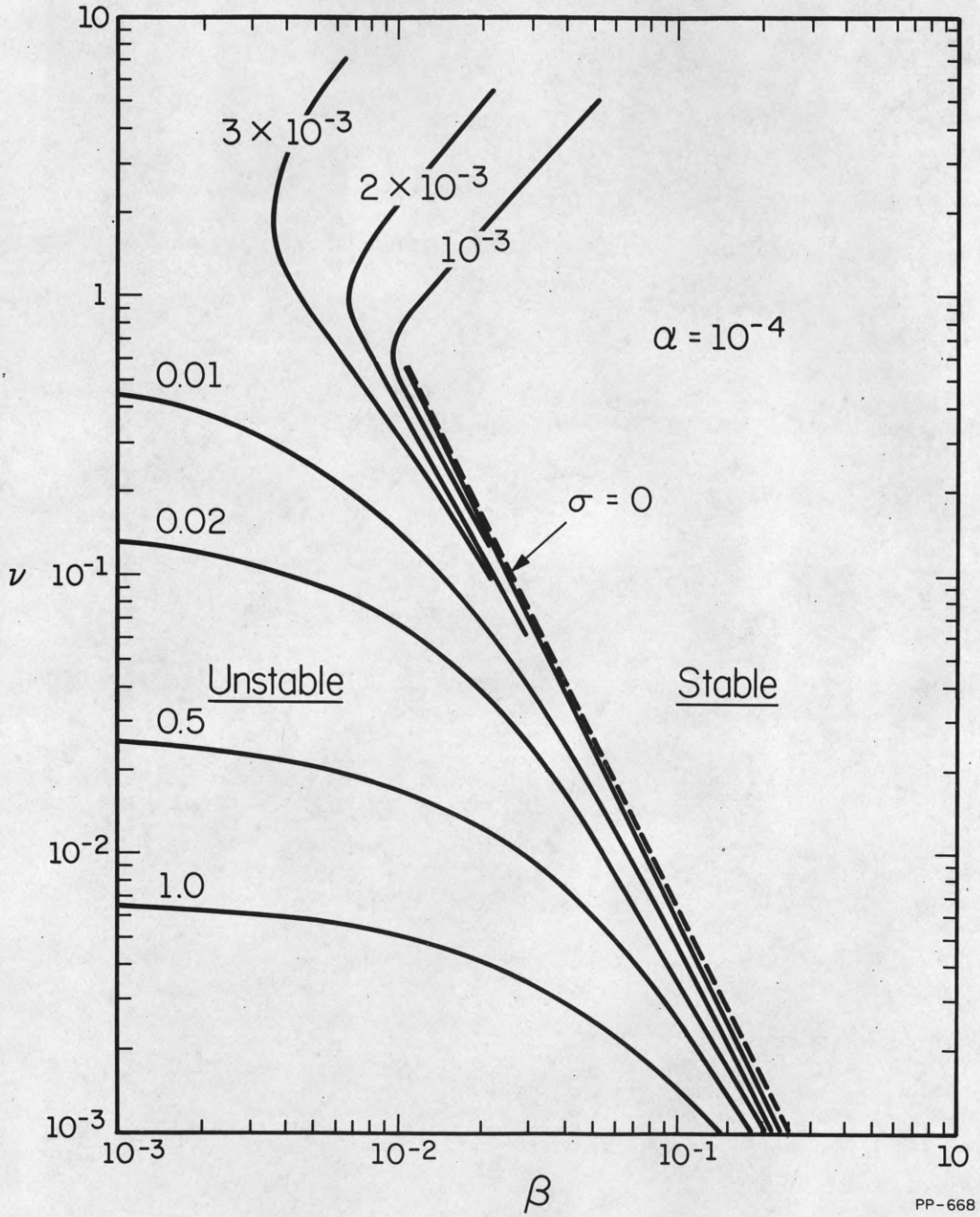

Figure 12. Contours of maximum spatial growth rate in a v-β-diagram. The parameters are the values of $\frac{\sigma v_o}{\omega p}$. The dashed line is the approximate expression of Equation 36.

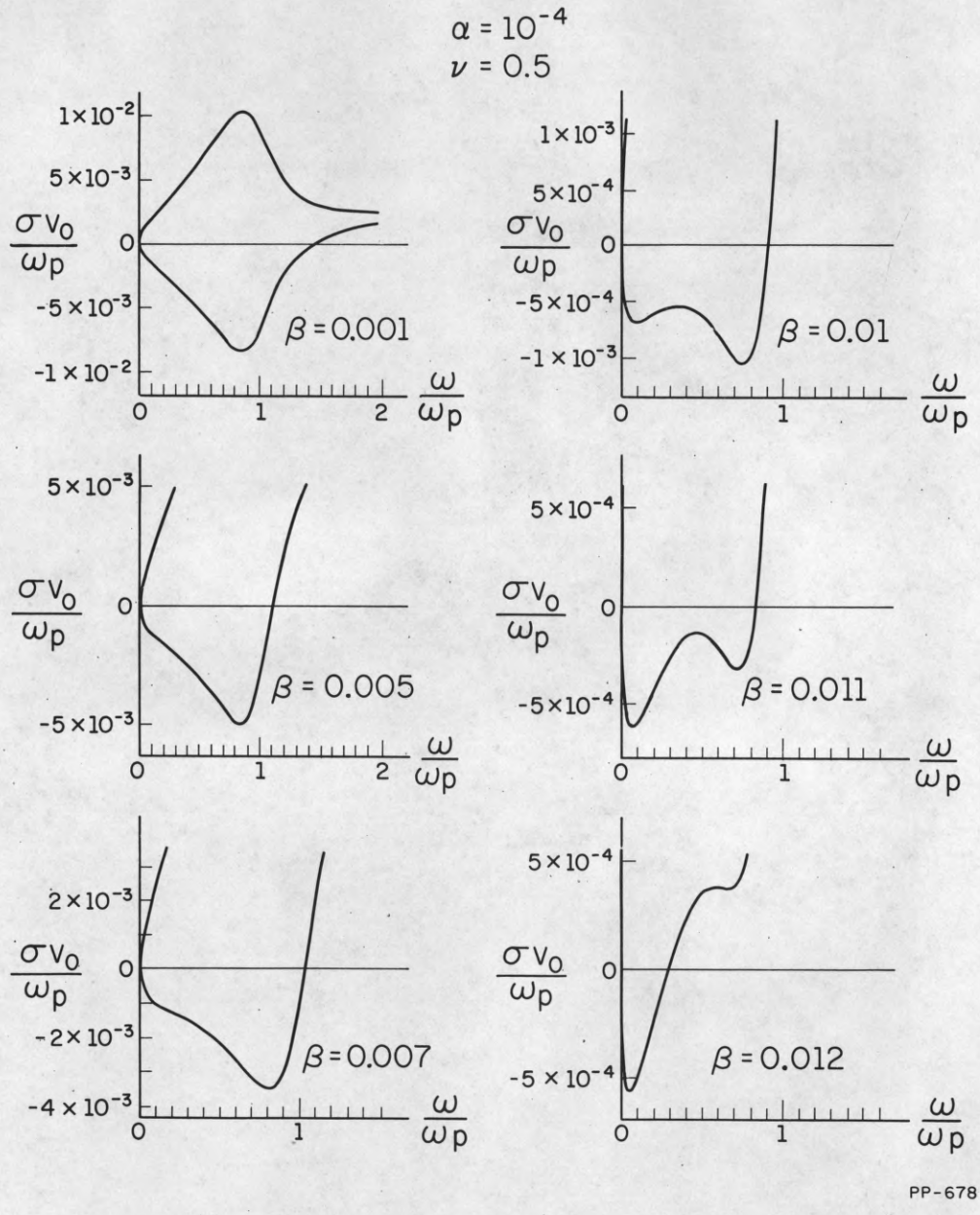

Figure 13. Spatial growth rate as a function of frequency for different velocity spreads at constant collision frequency. Instability corresponds to negative values of σ.

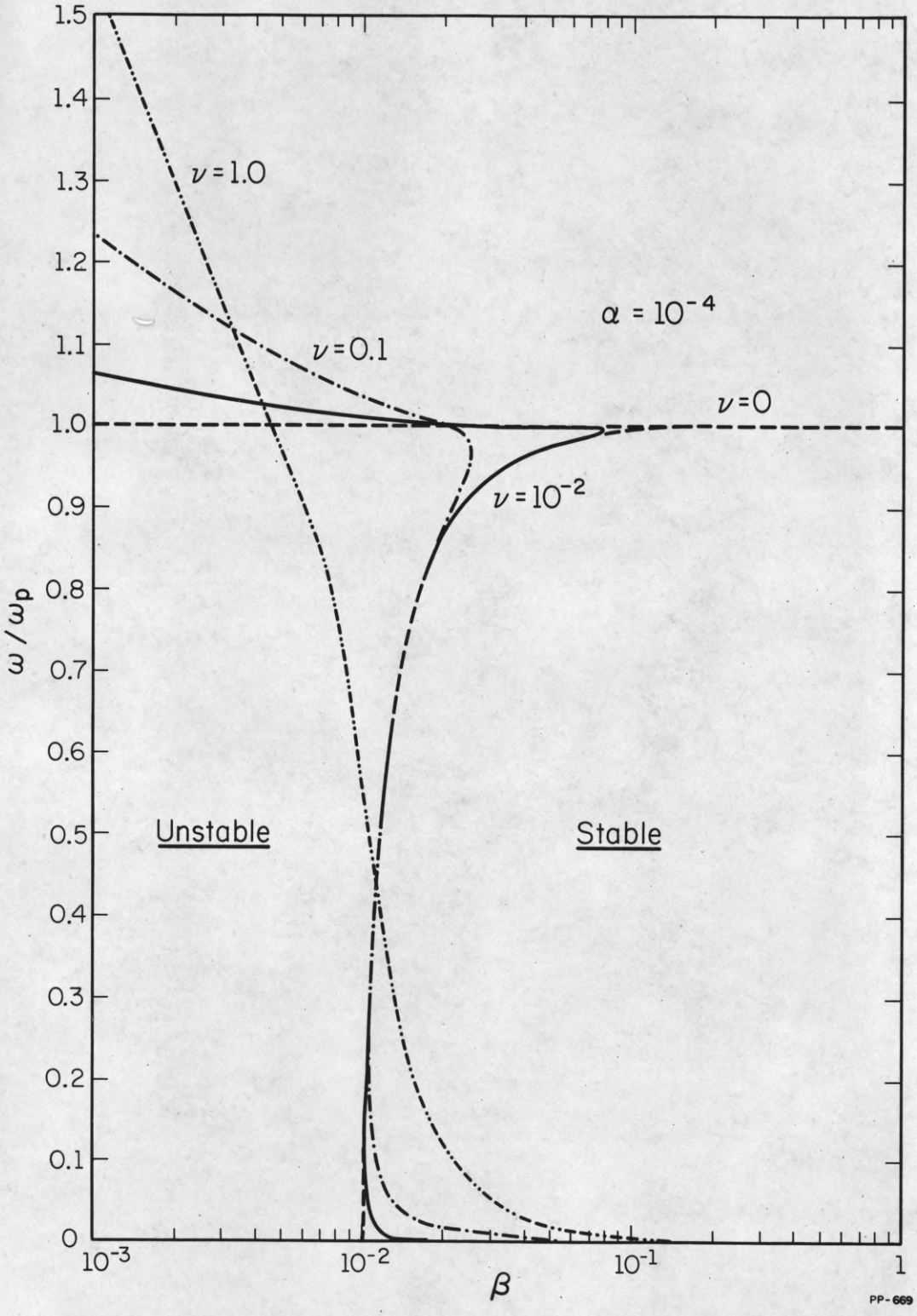

Figure 14. Contours of zero spatial growth rate in a ω-β-diagram.

(41) $$\frac{3^{\frac{1}{4}}}{2} (\alpha/2\nu)^{\frac{1}{2}} = \beta$$

This is again very nearly the same as the condition for quenching of the high frequency mode and valid for the same parameter range. It follows that in the region where the spatial growth is determined by collisions rather than plasma temperature, the instability is always of a non-resonant nature for real ω.

IV. GROUP VELOCITY AND RELATIONSHIP BETWEEN Im ω AND Im k

Under certain conditions the imaginary part of ω for real k and the imaginary part of k for real ω are connected by the relationship

(42) $$|\text{Im } \omega| = v_g |\text{ Im k }|$$

where $v_g = \frac{d\omega_r}{dk}$ is the group velocity of the unstable waves. This relation is frequently used in the literature to relate the temporal and the spatial growth of an instability[18-19]. The above stated relationship follows from the dielectric function

$$\epsilon (k,\omega) = o$$

by writing it

$$\epsilon(k,\omega) = \epsilon_r (k,\omega_r + i\, \omega_i) + i\, \epsilon_i (k,\omega_r + i\, \omega_i) = o$$

and expanding it into a Taylor series for small ω_i. One obtains to first order

(43) $$\omega_i = \frac{\epsilon_i(k,\omega_r)}{\partial\epsilon_r/\partial\omega \Big|_{\omega = \omega_r}} ; \qquad \epsilon_r(k,\omega_r) = 0$$

In the same manner one finds for $k = k_r + k_i$

(44) $$k_i = \frac{\epsilon_i(k_r,\omega)}{\partial\epsilon_r/\partial k \Big|_{k = k_r}}; \qquad \epsilon_r(k_r,\omega) = 0$$

and Equation 42 follows. For this relation to be valid it is necessary that the growth rate is determined by the imaginary part of the dielectric function which is proportional to the slope of the distribution function. This in turn implies that the interaction is resonant. For the beam instability the application of Equation 42 is therefore restricted to either the collisionless regime or, in the collision dominated regime, to the parameter region close to the instability limit.

To illustrate this point we have computed the group velocity for various collision frequencies as a function of the velocity spread of the beam and compared this with the ratio $\gamma_{opt}/\sigma_{opt}$ for the most unstable mode. The group velocities are plotted in Figure 15 and the ratio $\gamma_{opt}/\sigma_{opt}$ in Figure 16. We see that $\gamma_{opt}/\sigma_{opt}$ indeed approaches unity as the system approaches stability. For high collision frequencies the ratio also tends to unity, this, however, may be fortuitous.

Figure 17 shows a plot of the group velocity (computed for real k) of the unstable mode as a function of k for the same parameters as in Figure 7. It is interesting to note, that the dramatic variation of the group velocity over the unstable wavenumber range, which is associated with the change in mode structure, is not at all reflected in the group velocity of the most unstable mode as shown in Figure 15 which just exhibits a monotonic decrease with increasing β.

V. SUMMARY

A numerical and analytical study of the dispersion relation of a beam with finite velocity spread interaction with a cold plasma in the

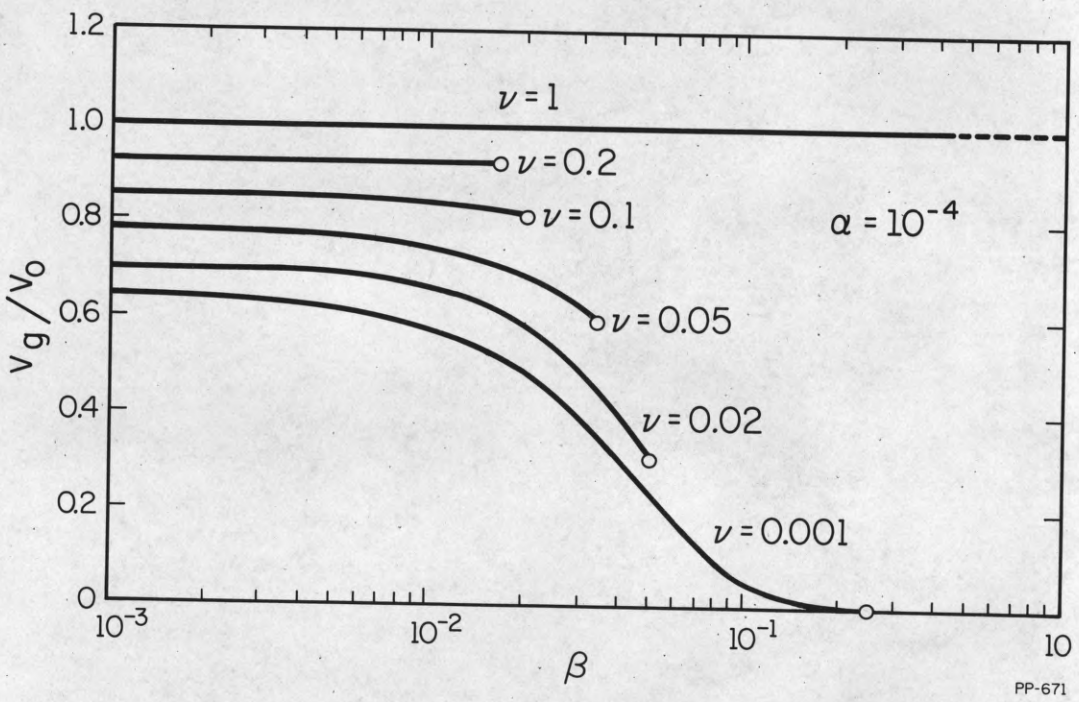

Figure 15. Group velocity of the most unstable mode as a function of velocity spread for different collision frequencies. The end points correspond to the stability limit.

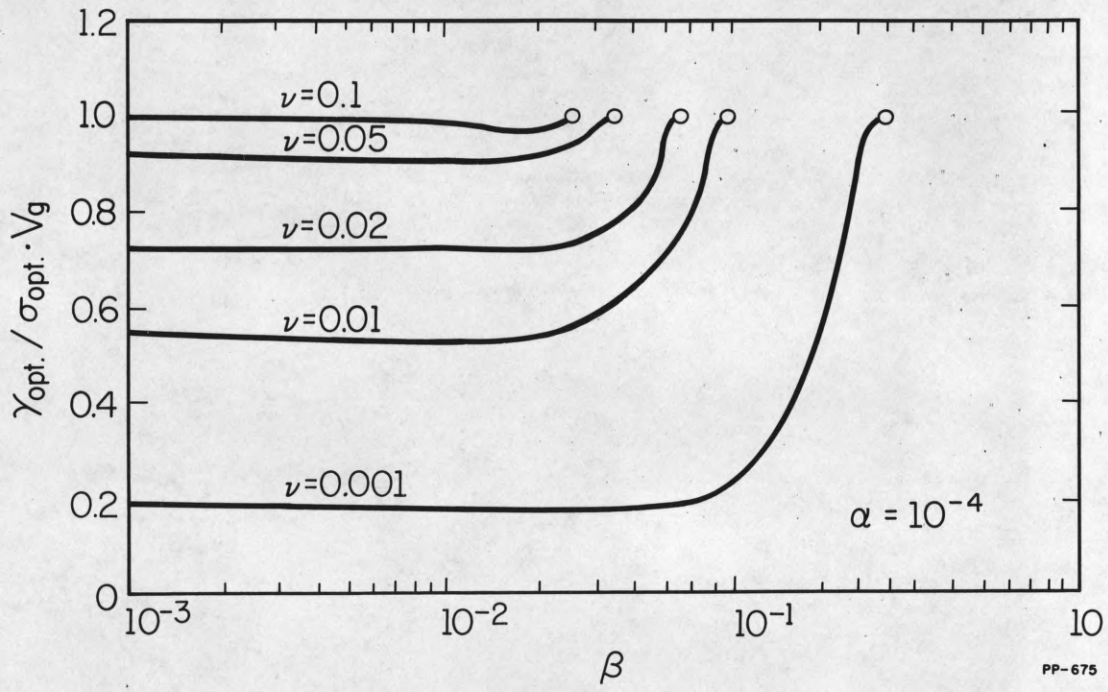

Figure 16. Ratio of $\gamma_{opt}/\sigma_{opt}\ v_g$ as a function of velocity spread for different collision frequencies.

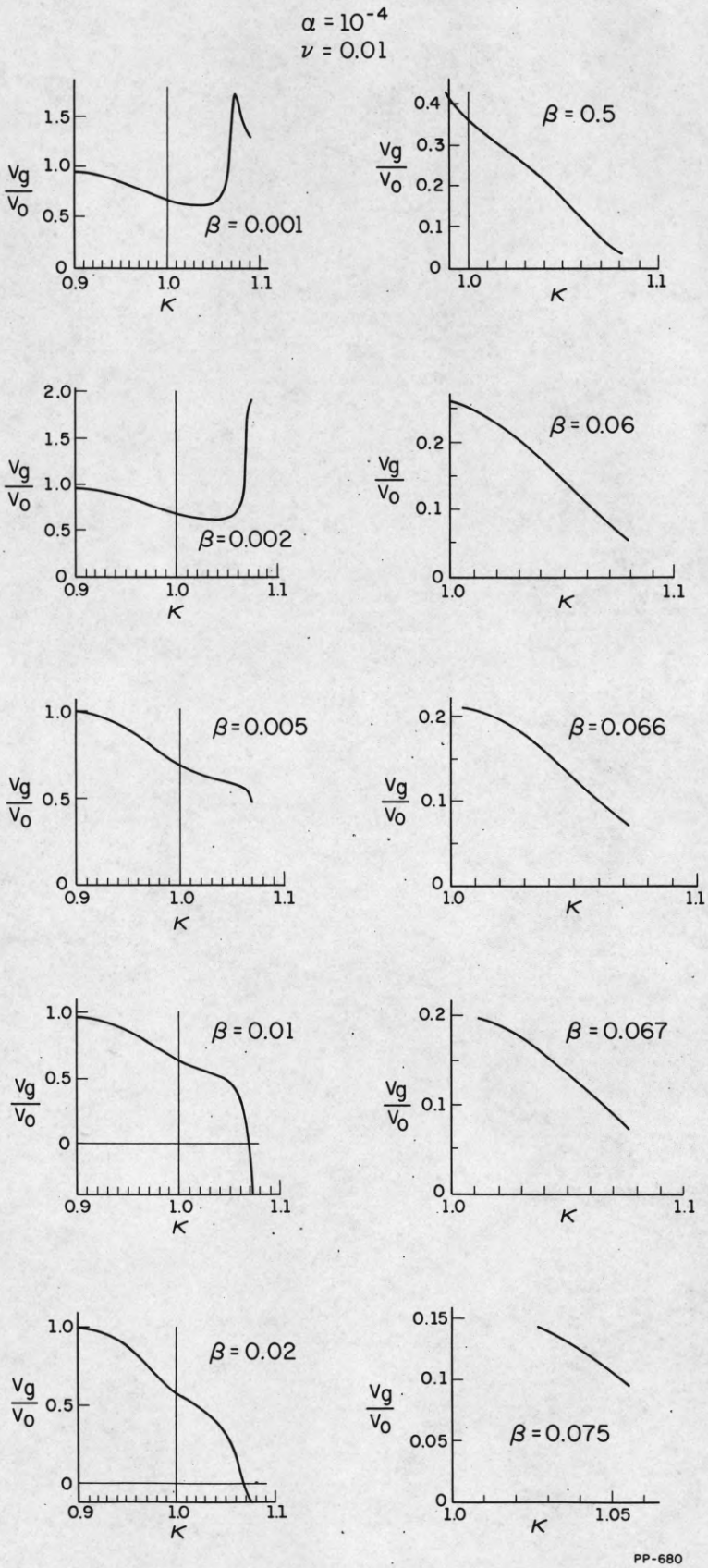

Figure 17. Group velocity of the unstable mode as a function of wave number for different velocity spreads.

presence of collisions, characterized by a constant collision frequency, allows the following general conclusions to be drawn.

(1) For a cold beam collisions tend to shift the wavenumber (frequency) of maximum instability towards lower values. In the limit of large collision frequency the instability becomes collision driven and the growth rate approaches a limiting constant value. The unstable root of the dispersion relation is associated with the slow-beam-branch.

(2) A velocity spread of the beam decreases the growth rate for sufficiently large velocity spread the unstable mode separates into a high and a low frequency mode. The instability of the high frequency mode is suppressed for collision frequencies larger than approximately α/β^2. The low frequency mode is always unstable but its growth rate becomes very small.

(3) For real wavenumber and a critical velocity spread, given approximately by $\beta \approx \frac{\nu}{2}$ the unstable mode switches over from the beam branch to the plasma branch of the dispersion relation.

(4) The presence of collisions changes the criterium for the interaction to be resonant or non-resonant. For real wavenumber resonant interaction occurs only for $\beta > \alpha^{1/3}$ and $\nu < \alpha^{1/3}$. For real frequency the interaction is always non-resonant provided that the spatial growth rate is limited by collisions rather than plasma temperature.

(5) In the non-resonant regime there is no general relationship between the spatial and the temporal growth rate except at high collision frequencies.

Acknowledgements

Thanks are due to Mrs. Virginia Metze for writing the computer program used in the numerical calculations and to Professor E. A. Jackson for many valuable comments and suggestions.

References

1) A. I. Akhiezer and Ya. B. Fainberg, Doklady Acad. Nauk SSR 69, 555, 1949.

2) D. Bohm and E. Gross, Phys. Rev. 75, 1967, 1949.

3) M. Sumi, J. Phys. Soc. Japan, 13, 1476, 1958; 14, 653 1959.

4) S. A. Bludman, K. M. Watson and M. N. Rosenbluth, Phys. Fluids 3, 747, 1960.

5) V. S. Imshennik and Yu. I. Morozov, Sov. Phys. Tech. Phys. 6, 464, 1961.

6) S. V. Yadavalli, J. Electron. Contr. 10, 437, 1961.

7) G. D. Boyd, R. W. Gould and L. M. Field, Proc. IRE 49, 1906, 1961.

8) G. Ascoli, University of Illinois, CSL Report R-131, 1961.

9) H. E. Singhaus, Phys. Fluids 7, 1534, 1964.

10) S. Ichimaru, Phys. Fluids 5, 1264, 1962.

11) T. Ohnuma and Y. Hatta, J. Phys. Soc. Japan, 21, 986 1965.

12) R. T. Briggs, Electron-Stream Interactions with Plasmas, MIT Press, 1964.

13) F. W. Crawford, Int. J. of Electronics 19, 217, 1965.

14) T. M. O'Neil and J. H. Malmberg, Phys. Fluids 11, 1754, 1968.

15) P. C. Clemmow, J. Plasma Phys. 2, 85, 1968.

16) M. N. Rosenbluth, Phys. Fluids 6, 932, 1960.

17) S. V. Yadavalli, Z. F. Physik, 196, 255, 1966.

18) W. E. Drummond, Phys. Fluids 7, 816, 1964.

19) Ya. B. Fainberg and V. D. Shapiro, Sov. Phys. JETP, 20, 937, 1965.

20) J. Chang, H. Böhmer, and M. Raether, Rev. Sci. Instr. 39, 1873, 1968.

21) H. Böhmer, J. Chang, and M. Raether, Plasma Physics, 11, 645, 1969.

Distribution List as of 1 October, 1969

Dr A.A. Dougal
Asst Director (Research)
Ofc of Defense Res & Eng
Department of Defense
Washington, D.C. 20301

Office of Deputy Director
(Research and Information, Rm 3D1037)
Department of Defense
The Pentagon
Washington, D.C. 20301

Director, Advanced Research Projects
Agency
Department of Defense
Washington, D.C. 20301

Director for Materials Sciences
Advanced Research Projects Agency
Department of Defense
Washington, D.C. 20301

Headquarters
Defense Communications Agency (340)
Washington, D.C. 20305

Defense Documentation Center
Attn: DDC-TCA
Cameron Station
Alexandria, Virginia 22314 (50 Copies)

Director
National Security Agency
Attn: TDL
Fort George G. Meade, Maryland 20755

Weapons Systems Evaluation Group
Attn: Colonel Blaine O. Vogt
400 Army-Navy Drive
Arlington, Virginia 22202

Central Intelligence Agency
Attn: OCR/DD Publications
Washington, D.C. 20505

Hq USAF (AFRDD)
The Pentagon
Washington, D.C. 20330

Hq USAF (AFRDDG)
The Pentagon
Washington, D.C. 20330

Hq USAF (AFRDSD)
The Pentagon
Washington, D.C. 20330

Colonel E.P. Gaines, Jr.
ACDA/FO
1901 Pennsylvania Ave N.W.
Washington, D.C. 20451

Lt Col R.B. Kalisch (SREE)
Chief, Electronics Division
Directorate of Engineering Sciences
Air Force Office of Scientific Research
Arlington, Virginia 22209

Dr I.R. Mirman
AFSC (SCT)
Andrews Air Force Base, Maryland 20331

AFSC (SCTSE)
Andrews Air Force Base, Maryland 20331

Mr Morton M. Pavane, Chief
AFSC Scientific and Technical Liaison Office
26 Federal Plaza, Suite 1313
New York, New York 10007

Rome Air Development Center
Attn: Documents Library (EMTLD)
Griffiss Air Force Base, New York 13440

Mr H.E. Webb (EMMIIS)
Rome Air Development Center
Griffiss Air Force Base, New York 13440

Dr L.M. Hollingsworth
AFCRL (CRN)
L.G. Hanscom Field
Bedford, Massachusetts 01730

AFCRL (CRMPLR), Stop 29
AFCRL Research Library
L.G. Hanscom Field
Bedford, Massachusetts 01730

Hq ESD (ESTI)
L.G. Hanscom Field
Bedford, Massachusetts 01730 (2 copies)

Professor J. J. D'Azzo
Dept of Electrical Engineering
Air Force Institute of Technology
Wright-Patterson AFB, Ohio 45433

Dr H.V. Noble (CAVT)
Air Force Avionics Laboratory
Wright-Patterson AFB, Ohio 45433

Director
Air Force Avionics Laboratory
Wright-Patterson AFB, Ohio 45433

AFAL (AVTA/R.D. Larson
Wright-Patterson AFB, Ohio 45433

Director of Faculty Research
Department of the Air Force
U.S. Air Force Academy
Colorado Springs, Colorado 80840

Academy Library (DFSLB)
USAF Academy
Colorado Springs, Colorado 80840

Director
Aerospace Mechanics Division
Frank J. Seiler Research Laboratory (OAR)
USAF Academy
Colorado Springs Colorado 80840

Director, USAF PROJECT RAND
Via: Air Force Liaison Office
The RAND Corporation
Attn: Library D
1700 Main Street
Santa Monica, California 90045

Hq SAMSO (SMTTA/Lt Nelson)
AF Unit Post Office
Los Angeles, California 90045

Det 6, Hq OAR
Air Force Unit Post Office
Los Angeles, California 90045

AUL3T-9663
Maxwell AFB, Alabama 36112

AFETR Technical Library
(ETV,MU-135)
Patrick AFB,Florida 32925

ADTC (ADBPS-12)
Eglin AFB, Florida 32542

Mr B.R. Locke
Technical Adviser, Requirements
USAF Security Service
Kelly Air Force Base, Texas 78241

Hq AMD (AMR)
Brooks AFB, Texas 78235

USAFSAM (SMKOR)
Brooks AFB, Texas 78235

Commanding General
Attn: STEWS-RE-L, Technical Library
White Sands Missile Range
New Mexico 88002 (2 copies)

Hq AEDC (AETS)
Attn: Library/Documents
Arnold AFS, Tennessee 37389

European Office of Aerospace Research
APO New York 09667

Phsical & Engineering Sciences Division
U.S. Army Research Office
3045 Columbia Pike
Arlington, Virginia 22204

Commanding General
U.S. Army Security Agency
Attn: IARD-T
Arlington Hall Station
Arlington, Virginia 22212

Commanding General
U.S. Army Materiel Command
Attn: AMCRD-TP
Washington, D.C. 20315

Technical Director (SMUFA-A2000-107-1)
Frankford Arsenal
Philadelphia, Pennsylvania 19137

Redstone Scientific Information Center
Attn: Chief, Document Section
U.S. Army Missile Command
Redstone Arsenal, Alabama 35809

Commanding General
U.S. Army Missile Command
Attn: AMSMI-REX
Redstone Arsenal, Alabama 35809

Commanding General
U.S. Army Strategic Communications Command
Attn: SCC-CG-SAE
Fort Huachuca, Arizona 85613

Commanding Officer
Army Materials and Mechanics Res. Center
Attn: Dr H. Priest
Watertown Arsenal
Watertown, Massachusetts 02172

Commandant
U.S. Army Air Defense School
Attn: Missile Science Division, C&S Dept
P.O. Box 9390
Fort Bliss, Texas 79916

Commandant
U.S. Army Command & General Staff College
Attn: Acquisitions, Library Division
Fort Leavenworth, Kansas 66027

Commanding Officer
U.S. Army Electronics R&D Activity
White Sands Missile Range, New Mexico 88002

Mr Norman J. Field, AMSEL-RD-S
Chief, Office of Science & Technology
Research and Development Directorate
U.S. Army Electronics Command
Fort Monmouth, New Jersey 07703

Commanding Officer
Harry Diamond Laboratories
Attn: Dr Berthold Altman (AMXDO-TI)
Connecticut Avenue and Van Ness St N.W.
Washington, D.C. 20438

Director
Walter Reed Army Institute of Research
Walter Reed Army Medical Center
Washington, D.C. 20012

Commanding Officer (AMXRD-BAT)
U.S. Army Ballistics Research Laboratory
Aberdeen Proving Ground
Aberdeen, Maryland 21005

Technical Director
U.S. Army Limited War Laboratory
Aberdeen Proving Ground
Aberdeen, Maryland 21005

Commanding Officer
Human Engineering Laboratories
Aberdeen Proving Ground
Aberdeen, Maryland 21005

U.S. Army Munitions Command
Attn: Science & Technology Br. Bldg 59
Picatinny Arsenal, SMUPA-VA6
Dover, New Jersey 07801

U.S. Army Mobility Equipment Research
and Development Center
Attn: Technical Document Center, Bldg 315
Fort Belvoir, Virginia 22060

Director
U.S. Army Engineer Geodesy,
Intelligence & Mapping
Research and Development Agency
Fort Belvoir, Virginia 22060

Dr Herman Robl
Deputy Chief Scientist
U.S. Army Research Office (Durham)
Box CM, Duke Station
Durham, North Carolina 27706

Richard O. Ulsh (CRDARD-IPO)
U.S. Army Research Office (Durham)
Box CM, Duke Station
Durham, North Carolina 27706

Mr Robert O. Parker, AMSEL-RD-S
Executive Secretary, JSTAC
U.S. Army Electronics Command
Fort Monmouth, New Jersey 07703

Commanding General
U.S. Army Electronics Command
Fort Monmouth, New Jersey 07703

Attention:AMSEL-SC
RD-GF
RD-MT
XL-D
XL-E
XL-C
XL-S (Dr R. Buser)
HL-CT-DD
HL-CT-R
HL-CT-L (Dr W.S. McAfee)
HL-CT-O
HL-CT-I
HL-CT-A
NL-D
NL-A
NL-P
NL-P-2 (Mr D. Haratz)
NL-R (Mr R. Kulinyi)
NL-S
KL-D
KL-E
KL-S (Dr H. Jacobs)
KL-SM (Drs Schiel/Hieslmair)
KL-T
VL-D
VL-P (Mr R.J. Niemela)
WL-D

1 copy to each symbol listed individually addressed

Dr A.D. Schnitzler, AMSEL-HL-NVII
Night Vision Laboratory, USAECOM
Fort Belvoir, Virginia 22060

Dr G.M. Janney, AMSEL-HL-NVOR
Night Vison Laboratory,USAECOM
Fort Belvoir, Virginia 22060

Atmospheric Sciences Office
Atmospheric Sciences Laboratory
White Sands Missile Range
New Mexico 88002

Missile Electronic Warfare,
Technical Area, AMSEL-WT-MT
White Sands Missile Range
New Mexico 88002

Project Manager
Common Positioning & Navigation Systems
Attn: Harold H. Bahr (AMCPM-NS-TM), Bldg 439
U.S. Army Electronics Command
Fort Monmouth, New Jersey 07703

Director, Electronic Programs
Attn: Code 427
Department of the Navy
Washington, D.C. 20360

Commander
U.S. Naval Security Group Command
Attn: G43
3801 Nebraska Avenue
Washington, D.C. 20390

Director
Naval Research Laboratory
Washington, D.C. 20390
Attn: Code 2027 6 copies
Dr W.C. Hall, Code 7000 1 copy
Dr A. Brodizinsky, Sup.Elec Div. 1 copy

Dr G.M.R. Winkler
Director, Time Service Division
U.S. Naval Observatory
Washington, D.C. 20390

Naval Air Systems Command
AIR 03
Washington, D.C. 20360 2 copies

Naval Ship Systems Command
Ship 031
Washington, D.C. 20360

Naval ship Systems Command
Ship 035
Washington, D.C. 20360

U.S. Naval Weapons Laboratory
Dahlgren, Virginia 22448

Naval Electronic Systems Command
ELEX 03, Room 2046 Munitions Building
Department of the Navy
Washington, D.C. 20360 (2 copies)

Commander
Naval Electronics Laboratory Center
Attn: Library
San Diego, California 92152 (2 copies)

Deputy Director and Chief Scientist
Office of Naval Research Branch Office
1030 Est Gree Street
Pasadena, California 91101

Library (Code2124)
Technical Report Section
Naval Postgraduate School
Monterey, California 93940

Glen A. Myers (Code 52Mv)
Assoc Professor of Elec. Engineering
Naval Postgraduate School
Monterey, California 93940

Commanding Officer and Director
U.S. Naval Underwater Sound Laboratory
Fort Trumbull
New London, Connecticut 06840

Commanding Officer
Naval Avionics Facility
Indianapolis, Indiana 46241

Dr H. Harrison, Code RRE
Chief, Electrophysics Branch
National Aeronautics & Space Admin.
Washington, D.C. 20546

NASA Lewis Research Center
Attn: Library
21000 Brookpark Road
Cleveland, Ohio 44135

Los Alamos Scientific Laboratory
Attn: Report Library
P.O. Box 1663
Los Alamos, New Mexico 87544

Federal Aviation Administration
Attn: Admin Stds Div (MS-110)
800 Independence Ave S.W.
Washington, D.C. 20590

Head, Technical Services Division
Naval Investigative Service Headquarters
4420 North Fairfax Drive
Arlington, Virginia 22203

Commander
U.S. Naval Ordnance Laboratory
Attn: Librarian
White Oak, Maryland 21502 (2 copies)

Commanding Officer
Office of Naval Research Branch Office
Box 39 FPO
New York, New York 09510

Commanding Officer
Office of Naval Research Branch Office
219 South Dearborn Street
Chicago, Illinois 60604

Commanding Officer
Office of Naval Research Branch Office
495 Summer Street
Boston, Massachusetts 02210

Commander (ADL)
Naval Air Development Center
Johnsville, Warminster, Pa 18974

Commanding Officer
Naval Training Device Center
Orlando, Florida 32813

Commander (Code 753)
Naval Weapons Center
Attn: Technical Library
China Lake, California 93555

Commanding Officer
Naval Weapons Center
Corona Laboratories
Attn: Library
Corona, California 91720

Commander, U.S. Naval Missile Center
Point Mugu, California 93041

W.A. Eberspacher, Associate Head
Systems Integration Division
Code 5340A, Box 15
U.S. Naval Missile Center
Point Mugu, California 93041

Mr M. Zane Thornton, Chief
Network Engineering, Communications
and Operations Branch
Lister Hill National Center for
Biomedical Communications
8600 Rockville Pike
Bethesda, Maryland 20014

U.S. Post Office Department
Library - Room 1012
12th & Pennsylvania Ave, N.W.
Washington, D.C. 20260

Director
Research Laboratory of Electronics
Massachusetts Institute of Technology
Cambridge, Massachusetts 02139

Mr Jerome Fox, Research Coordinator
Polytechnic Institute of Brooklyn
55 Johnson Street
Brooklyn, New York 11201

Director
Columbia Radiation Laboratory
Columbia University
538 West 120th Street
New York, New York 10027

Director
Coordinated Science Laboratory
University of Illinois
Urbana, Illinois 61801

Director
Stanford Electronics Laboratories
Stanford University
Stanford, California 94305

Director
Microwave Physics Laboratory
Stanford University
Stanford, California 94305

Director, Electronics Research Laboratory
University of California
Berkeley, California 94720

Director
Electronic Sciences Laboratory
University of Southern California
Los Angeles, California 90007

Director
Electronics Research Center
The University of Texas at Austin
Austin Texas 78712

Division of Engineering and Applied Physics
210 Pierce Hall
Harvard University
Cambridge, Massachusetts 02138

Dr G.J. Murphy
The Technological Institute
Northwestern University
Evanston, Illinois 60201

Dr John C. Hancock, Head
School of Electrical Engineering
Purdue University
Lafayette, Indiana 47907

Dept of Electrical Engineering
Texas Technological College
Lubbock, Texas 79409

Aerospace Corporation
P.O. Box 95085
Los Angeles, California 90045
Attn: Library Acquisitions Group

Proffessor Nicholas George
California Inst of Technology
Pasadena, California 91109

Aeronautics Library
Graduat Aeronautical Laboratories
California Institute of Technology
1201 E. California Blvd
Pasadena, California 91109

The John Hoplins University
Applied Physics Laboratory
Attn: Document Librarian
8621 Georgia Avenue
Silver Spring, Maryland 20910

Raytheon Company
Attn: Librarian
Bedford, Massachusetts 01730

Raytheon Company
Research Division Library
28 Seyon Street
Waltham, Massachusetts 02154

Dr Sheldon J. Wells
Electronic Properties Information Center
Mail Station E-175
Hughes Aircraft Company
Culver City, California 90230

Dr Robert E. Fontana
Systems Research Laboratories Inc.
7001 Indian Ripple Road
Dayton, Ohio 45440

Nuclear Instrumentation Group
Bldg 29, Room 101
Lawrence Radiation Laboratory
University of California
Berkeley, California 94720

Sylvania Electronic Systems
Applied Research Laboratory
Attn: Documents Librarian
40 Sylvan Road
Waltham, Massachusetts 02154

Hollander Associates
P.O. Box 2276
Fullerton, California 92633

Illinois Institute of Technology
Dept of Electrical Engineering
Chicago, Illinois 60616

The University of Arizona
Dept of Electrical Engineering
Tucson, Arizona 85721

Utah State University
Dept Of Electrical Engineering
Logan, Utah 84321

Case Institute of Technology
Engineering Division
University Circle
Cleveland, Ohio 44106

Hunt Library
Carnegie-Mellon University
Schenley Park
Pittsburgh, Pennsylvania 15213

Dr Leo Youns
Stanford Research Institute
Menlo Park, California 94025

School of Engineering Sciences
Arizona State University
Tempe, Arizona 85281

Engineering & Mathmatical Sciences Library
University of California at Los Angeles
405 Hilgred Avenue
Los Angeles, California 90024

The Library
Government Publications Section
University of California
Santa Barbara, California 93106

Carnegie Institute of Technology
Electrical Engineering Department
Pittsburgh, Pennsylvania 15213

Professor Joseph E. Rowe
Chairman, Dept of Electrical Engineering
The University of Michigan
Ann Arbor, Michigan 48104

New York University
College of Engineering
New York, New York 10019

Syracuse University
Dept of Electrical Engineering
Syracuse, New York 13210

Yale University
Engineering Department
New Haven, Connecticut 06520

Airborne Instruments Laboratory
Deerpark, New York 11729

Raytheon Company
Attn: Librarian
Bedford, Massachusetts 01730

Lincoln Laboratory
Massachusetts Institute of Technology
Lexington, Massachusetts 02173

The University of Iowa
The University Libraries
Iowa City, Iowa 52240

Lenkurt Electric Co,Inc
1105 County Road
San Carlos, California 94070
Attn: Mr E.K. Peterson

Philco Ford Corporation
Communications & Electronics Div.
Union Meeting and Jolly Rods
Blue Bell, Pennsylvania 19422

Union Carbide Corporation
Electronic Division
P.O. Box 1209
Mountain View, California 94041

Electromagnetic Compatibility Analysis Center
(ECAC), Attn: ACLP
North Severn
Annapolis, Maryland 21402

Director
U. S. Army Advanced Materiel Concepts Agency
Washington, D.C. 20315

ERRATUM

Mr Jerome Fox, Research Coordinator
Polytechnic Institute of Brooklyn
55 Johnson St (Should be 333 Jay St)
Brooklyn, N.Y. 11201

DELETE

Mr Morton M. Pavane, Chief
AFSC Scientific & Tech. Liaison Office
26 Federal Plaza, Suite 1313
New York, N. Y. 10007

Commanding Officer
Office of Naval Research Branch Office
Box 39 FPO
New York, N. Y. 09510

ADDENDUM

Dept of Electrical Engineering
Rice University
Houston, Texas 77001

Research Laboratories for the Eng. Sc.
School of Engineering & Applied Science
University of Virginia
Charlottesville, Virginia 22903

Dept of Electrical Engineering
College of Engineering & Technology
Ohio University
Athens, Ohio 45701

Project Mac
Document Room
Massachusetts Institute of Technology
545 Technology Square
Cambridge, Massachusetts 02139

Lehigh University
Dept of Electrical Engineering
Bethelhelm, Pennsylvania 18015

Commander Test Command (TCD-)
Defense Atomic Support Agency
Sandia Base
Albuquerque, New Mexico 87115

Materials Center Reading Room 13-2137
Massachusetts Institute of Technology
Cambridge, Massachusetts 02139

Professor James A. Cadzow
Department of Electrical Engineering
State University of New York at Buffalo
Buffalo, New York 14214

Director, Naval Research Laboratory
Attn: Library, Code 2029 (ONRL)
Washington, D.C. 20390

Commanding Officer (Code 2064)
Navy Underwater Sound Laboratory
Fort Trumbull
New London, Connecticutt 06320

Security Classification

DOCUMENT CONTROL DATA - R & D

(Security classification of title, body of abstract and indexing annotation must be entered when the overall report is classified)

1. ORIGINATING ACTIVITY *(Corporate author)* University of Illinois Coordinated Science Laboratory Urbana, Illinois 61801	2a. REPORT SECURITY CLASSIFICATION 2b. GROUP

3. REPORT TITLE

INFLUENCE OF COLLISIONS ON THE INSTABILITY OF AN ELECTRON BEAM IN A PLASMA

4. DESCRIPTIVE NOTES *(Type of report and inclusive dates)*

5. AUTHOR(S) *(First name, middle initial, last name)*

RAETHER, M.

6. REPORT DATE	7a. TOTAL NO. OF PAGES	7b. NO. OF REFS
November, 1969	36	21

8a. CONTRACT OR GRANT NO. DAAB 07-67-C-0199 b. PROJECT NO. c. d.	9a. ORIGINATOR'S REPORT NUMBER(S) R-445 9b. OTHER REPORT NO(S) *(Any other numbers that may be assigned this report)*

10. DISTRIBUTION STATEMENT

This Document has been approved for public release and sale; its distribution is unlimited.

11. SUPPLEMENTARY NOTES	12. SPONSORING MILITARY ACTIVITY
	Joint Services Electronics Program thru U.S. Army Electronics Command Fort Monmouth, New Jersey 07703

13. ABSTRACT

This report contains a numerical and analytical study of the dispersion relation of a Lorentzian beam in a cold plasma with collisions. Numerical results for the growth rate, the mode structure and the group velocity are presented for selected parameters analytical generalizations of these results are given, both for the case of real wavenumber and real frequency. In particular it is shown that in either case the high frequency instability is quenched for a sufficiently large velocity spread and collision frequency and that this quenching occurs over a much larger parameter range than has previously been assumed.

DD FORM 1 NOV 65 1473

Security Classification

14 KEY WORDS	LINK A		LINK B		LINK C	
	ROLE	WT	ROLE	WT	ROLE	WT
Beam Instability						
Collisions						
Dispersion Relations						
Numerical Solutions						
Resonant Interaction						